IEEE Access
Multidisciplinary | Rapid Review | Open Access Journal

Received April 6, 2021, accepted April 14, 2021, date of publication April 20, 2021, date of current version April 28, 2021.

Digital Object Identifier 10.1109/ACCESS.2021.3074351

SWIPT Model Adopting a PS Framework to Aid IoT Networks Inspired by the Emerging Cooperative NOMA Technique

THANH-NAM TRAN[1,2], THOAI PHU VO[3], PEPPINO FAZIO[1], AND MIROSLAV VOZNAK[1], (Senior Member, IEEE)

[1]Faculty of Electrical Engineering and Computer Science, Technical University of Ostrava, 70800 Ostrava, Czech Republic
[2]Faculty of Electronics and Telecommunications, Saigon University, Ho Chi Minh City 700000, Vietnam
[3]Faculty of Electrical and Electronics Engineering, Ton Duc Thang University, Ho Chi Minh City 700000, Vietnam

Corresponding author: Thoai Phu Vo (vophuthoai@tdtu.edu.vn)

This work was supported in part by the Ministry of Education, Youth and Sports under Grant SP2021/25, and in part by the Large Infrastructures for Research, Experimental Development and Innovations under Project LM2018140.

ABSTRACT We present the design for an ultra-low latency and low energy Internet of Things (IoT) network inspired by the emerging cooperative Non-Orthogonal Multiple Access (NOMA) wireless communication technique. The IoT network model consists of a source at the center of the network, a near device inside the network, and a far device outside the network. The far device is in the near proximity of the near device, however. We deploy the near device as a relay to assist the far device. The near device is assumed to be a low energy node. As a result, the near device cannot forward signals to the far device through its own power. We therefore design the IoT network to apply the Simultaneous Wireless Information and Power Transfer (SWIPT) technique so that the near device would be able to harvest energy and use it to forward signals. Two cooperative IoT network scenarios are examined: Half-Duplex (HD) and Full-Duplex (FD) relaying, each with and without eavesdroppers. The design also exploits Power Splitting (PS) factors for fairness in Quality of Service (QoS) for the devices. Novel analysis expressions are obtained accuracy and approximation of closed-forms for Outage Probability (OP), secrecy OP, system throughput and Jain's fairness index. The analysis results are proved and verified by Monte Carlo simulation results.

INDEX TERMS NOMA, SWIPT, EH, power splitting, fairness in QoS.

I. INTRODUCTION

A. BACKGROUND AND RELATED WORKS

Networked devices such as vehicular and wearable devices number in the billions and form Vehicle-to-Vehicle (V2V), Vehicle-to-Everything (V2X) and IoT networks [1]–[4]. The major challenge in practical IoT networks is serving multiple devices which consume less power while maintaining the required QoS [5]. IoT networks require a large amount of data to be delivered to terminal devices. The technical NOMA demonstrates promising use for future wireless communication networks through its effective spectrum sharing and ability to allocate different Power Allocation (PA) factors in the same power domain [6]–[8]. Wireless network performance depends on power resource allocation strategies. Ding *et al.* [9] investigated a NOMA network with random multiple user equipment (UE) and allocated PA factors for users according to the number of UE which join the network. Tran *et al.* [10] allocated PA factors for UE based on the mean of the Channel State Information (CSI) statistic. Timotheou and Krikidis examined fairness of QoS for UE in [11]. The authors verified that system performance depends on power resource allocation. If allocated PA factors for the users in network are not suitable, the OP performances at the users therefore may lead to one. 5G wireless communication networks must have much higher bit-rates ($100\times \sim 1000\times$ compared to 4G networks), lower latency (1 ms for a transmission block), massive connections (106 devices/Km^2 with diverse QoS requirements) [12], [13]. Compared to the benefits of the Orthogonal Multiple Access (OMA) technique, the NOMA technique is designed to share Degree-of-Freedom (DoF) between IoT devices with superposition coding and consequently must employ Multiple User Detection (MUD) to separate interfered UEs which share

The associate editor coordinating the review of this manuscript and approving it for publication was Yanjiao Chen.

the same DoF [12]. The NOMA technique benefits a large number of connections by allocating different PA factors in the same DoF. The NOMA technique may therefore provide greater overloading transmission and further significantly improve network capacity, wherein multiple devices with different traffic requirements may be multiplexed to transmit on the same DoF to improve latency and fairness. A comparison of OMA and NOMA is detailed in [12].

Energy Efficient (EE) performance was studied in [14], [15]. The authors investigated a Device-to-Device (D2D) model based on Energy Harvesting (EH) in which both pairing devices harvested energy from a Hybrid Access Point (HAP). The authors proposed an iterative algorithm to exploit optimal power control and time allocation [14]. In our work [16], we investigated a cooperative NOMA network and implemented various forwarding protocols such as Decode-and-Forward (DF) and Amplify-and-Forward (AF) with Fixed Gain (FG) or Variable Gain (VG) to optimize EE performance in Green-Wireless Networks (G-WNs).

Many technologies have been proposed to improve system performance: relaying to combat channel fading [17], multiple relays deployed to combine relay selection [18]–[20], signal forwarding using AF with FG [21] or AF with VG [22] instead of the DF protocol, channel gain modeling over Nakagami-*m* distributions [23], and Multiple-Input-Multiple-Output (MIMO) instead of Single-Input-Single-Output (SISO) [16], etc.

The NOMA technique enables billions of IoT devices to be served [24]–[26]. Superposition Coding (SC), which is employed in the NOMA scheme, is deployed at the Base Station (BS) to allocate different PA factors to IoT devices in the same power domain. IoT devices eliminate interference by utilizing Successive Interference Cancellation (SIC) [27].

A disadvantage of IoT devices (e.g., wearable devices) is their limited energy storage and battery power. IoT devices are not fixed in position nor directly supplied by the power grid. We investigated how to guarantee QoS in IoT devices under these conditions. A scheme for a wireless EH was recently described in [28]–[30]. The Radio Frequency (RF) EH technique was deployed because of its uninterrupted efficiency for WSNs and electronic harvesting circuit design [31].

B. MOTIVATION AND CONTRIBUTIONS

In green-Wireless Networks (g-WNs) which make use of Wireless Sensor Networks (WSNs), network nodes are deployed in a complex terrain which may not have a powered grid. The networked nodes are supplied with energy from renewable sources (solar, wind, etc.) to keep them active. SWIPT is a promising solution for low-powered IoT networks where the lifespan of IoT devices may be extended by simultaneously receiving wireless energy and information. Networked nodes may especially be served simultaneously without any delays since the information in networked nodes is superimposed in the signal. In an initial study of SWIPT and NOMA techniques, Yang *et al.* [32] investigated an HD-NOMA combining SWIPT with a fixed PS factor. Although the authors made significant contributions, some issues are still open and require investigations as:

- How the system performance is affected by different PS factors;
- How the system performance is affected if the relay functions in FD instead of HD mode;
- Whether harvested energy can be used to forward signals;
- Which PS factor is suitable for harvesting energy to forward signals under a constrained QoS for devices in an IoT network.

PLS in wireless communications is used especially to combat eavesdroppers. The risk of eavesdroppers is due to opportunistic broadcasting in wireless signals. Many security solutions have been proposed to improve security while information passes over a network: multi-relaying and best relay selection [35]–[37], equipped multi-antennae [38] combined multi-antennae and TAS protocol [39]–[42], signals distributed over Nakagami-*m* fading channels [43], optimized PA factors [44], secrecy performance in combination with SWIPT [45], [46], etc. To the best of our knowledge, no studies have investigated how to improve secrecy performance based on the PS factor.

Rabie *et al.* [47] examined the dual-hop relay network with a source, a relay and a destination. both Time Switching (TS) and PS protocols were deployed and obtained OP and ergodic capacity in closed-forms. The authors confirmed that the good selection of the EH time in TS protocol and PS factor in PS protocol was the primary key to reach the best system performance.

In another similarly work, it is interesting that the authors clearly analyzed TS and PS protocols in EH over cooperative wireless systems, where multiple relays assist a single destination [48]. Chen *et al.* [49] proposed the use of harvested power at the source to forward signals to the destination. However, we apply some "extended" issues:

- We consider how the network may simultaneously serve while the network contains multiple devices;
- And, we consider how PS factors may be used to combat eavesdroppers.

Inspired by the major previous studies, the following issues remain open and are addressed in our study:

- This study propose a low energy IoT network underlay cooperative NOMA technique, inspired by a major study [29]. The work in this study, however, investigate the effect of PS factors to the system performance of IoT network as the first aim;
- To improve system throughput of IoT network, the relay in this study adopts FD mode to reach ultra-low latency as the second aim;
- Our proposal assumes that the near device, specified as a relay, does not have power resources to forward a signal. We therefore suggest a novel SWIPT model that

uses harvested energy for the relay to forward signals as the third aim. In particular, instead of a fixed PS factor, We deploy an Additive PS factor with a constraint Signal-to-Interference-plus-Noise Ratio (SINR) achieved at the far device and approximately achieved SINR at the relay to ensure QoS fairness at the far device as the third aim. We thus obtain a novel OP at the device in terms of accuracy and approximate closed-forms as the contribution of this study;

- PLS has acknowledged one of the most issues in wireless communication networks. To our best knowledge, we consider exploiting an adaptive PS factor that may improve secrecy performance.

The paper is structured as follows: Section II describes the system models in detail; the system models are designed and formulated according to two IoT network schemes, with HD and FD scenarios. Section III provides an analysis of the system performance of two IoT networks. Section IV provides an analysis and the simulation results of two IoT network models. Section V presents a summary and conclusion of this study.

II. SYSTEM MODELS

Our study examines two individual down-link scenarios: SWIPT underlay HD/FD relay, and secrecy SWIPT underlay HD/FD relay.

A. CONCEPT AND FORMULATION OF AN UNDERLAY IoT NETWORK WITH HD RELAYING

The authors in [50] considered that cellular technologies contained disadvantages for IoT networks, allowing only a few devices to directly connect to each small-cell BS while providing wide bandwidth. This is the opposite of what is required by IoT devices, where a large number of sensor nodes need only sufficient bandwidth to transmit a few bytes every few minutes. This makes large-scale techniques impossible to be practiced without increasing costs and energy consumption. The authors in [50] proposed LoRa-based private networks for IoT applications. However, the IoT network model in our study plotted a part of the IoT which consisted of a gateway (source S) and two end nodes (devices D_1 and D_2). It is important to note the difference to the study [50]. In our study, we adopted the NOMA technique for private IoT networks. With the benefits of NOMA technique, our system model can serve multiple devices simultaneously. The NOMA technique has a better bandwidth allocation strategy because the devices share the spectrum in the same power domain. We also consider how IoT networks may be deployed in complex terrain where is difficult to supply power. By deploying the SWIPT technique, we hypothesized that private IoT networks could use RF-EH for to forward signals to the far end node (device D_2). Through the formulations and investigated results, we provide an interesting point-of-view for future IoT applications.

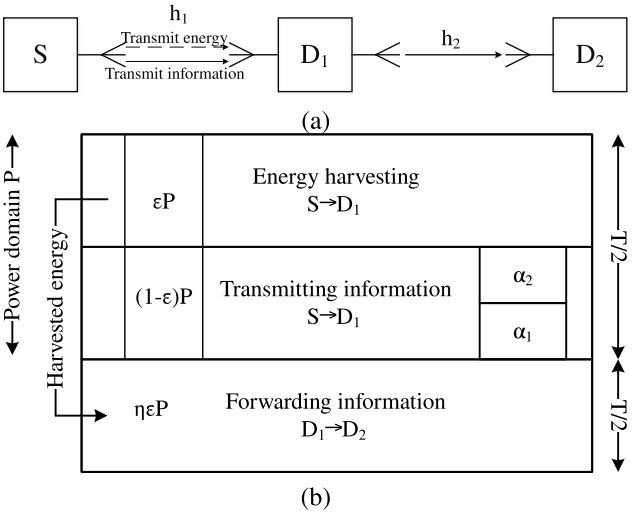

FIGURE 1. (a) An HD-IoT network underlay cooperative NOMA in combination with SWIPT; (b) PS diagram with HD relaying.

For clarity, the IoT network model depicted in Figure 1a has a source S and two devices D_1 and D_2. The source S at the center cell covers a certain area. The device D_1 is inside a certain area. However, we assume that device D_2 is outside the coverage area of source S. Therefore, no direct down-link from source S to device D_2 exists. Device D_2 broadcasts to assist synchronization (SYN) with the devices nearby. In this case, device D_1 receives the SYN requirement of device D_2 and replies with an acknowledgment (ACK) to device D_2. Device D_2 sends a finish (FIN) message to accept cooperation from device D_1. Device D_1 is thus implemented as a relay to assist device D_2. This study assumes that device D_1 fully sends its own CSI as feedback and the CSI from device D_2 to source S.

Two SWIPT techniques can be used: TS and PS. In [31], the authors fully presented RF EH. The authors also adopted and compared TS and PS protocols [47], [48]. The authors presented the TS diagrams in [47, Figure 2a] and [48, Figure 1b]. We observed that the previous TS diagrams required three time slots to complete a transmission block. The authors also presented the PS diagrams in [47, Figure 3a] and [48, Figure 3b]. We observed that the previous PS diagrams required two time slots to complete a transmission block. We also observed that the PS protocols provided greater network capacity than the TS protocols. The present study therefore applies the PS protocol, which is suitable for low latency and low energy IoT networks. Figure 1b illustrates different EH and signal processing through the deployment of the PS protocol compared to the previous PS diagrams in [47, Figure 3a] and [48, Figure 3b]. Note that the PS diagram (1b) with three tiers uses two time slots to complete a transmission block T according to [29], [32], [48]. In the first half of the transmission block, the BS transmits wireless energy (tier 1) and information (tier 2) simultaneously to device D_1. In terms of SWIPT using a PS protocol, a portion of the power domain P from the source is used

during the first half of the time block for EH, while the remaining portion is used for information processing. The ratio of EH is determined according to the PS factor ε. Therefore, εP is used for EH, and the remaining $\xi P = (1-\varepsilon)P$ is used for information processing at device D_1, where $0 \leq \varepsilon \leq 1$. EH architecture was presented in [31, Figure 4c] and [48, Figure 4]. In the second half of the transmission bock, device D_1 forwards information to D_2 by using the harvested energy (tier 1) and applying the DF protocol.

Source S fully owns the CSI of near device D_1 and far device D_2. We assume a single transmitting antenna and single receiving antenna at each node. In terms of cooperative NOMA theories by applying SC, source S superimposes the messages x_1 and x_2 of devices D_1 and D_2 into a signal and transmits it to the terminal devices. In cooperative networks, the BS have to select the relay for forwarding signals [18]–[20], [51]. In this study, the source S transmits the superimposed signal to the near device D_1. As a result, the received signal at near device D_1 is expressed as:

$$y_1^{(HD)} = h_1\sqrt{\xi^{(HD)}P}\left(\sqrt{\alpha_1}x_1 + \sqrt{\alpha_2}x_2\right) + n_1, \quad (1)$$

where PS factors $\varepsilon^{(HD)}$ and $\xi^{(HD)}$ are used for transmitting wireless energy and information, respectively, and $\xi^{(HD)} + \varepsilon^{(HD)} = 1$. h_1 is the fading channel from source S to near device D_1. Note that fading channel h_1 is modeled according to a Rayleigh fading channel such that $h_1 = d_1^{-\omega}$, where d_1 and ω are the distance $S \rightarrow D_1$ and path-loss exponent, respectively. The coefficient P is the power domain at source S. The devices share the spectrum in the same power domain P. Therefore, the messages x_1 and x_2 of the devices D_1 and D_2 are superimposed according to different PA factors α_1 and α_2. As shown in Figure 1, with constraint distance $S \rightarrow D_1$ being less than distance $S \rightarrow D_2$, we obtain the PA factor rule $\alpha_1 < \alpha_2$ and $\alpha_1 + \alpha_2 = 1$. n_1 is the Additive White Gaussian Noise (AWGN) such that $n_1 \sim (0, N_0)$, with zero mean and variance N_0.

After receiving the signal according to (1), the near device D_1 implements SIC to detect its own message x_1. However, $\alpha_1 < \alpha_2$ are constrained in this study. Therefore, the near device D_1 must decode the message x_2 of the far device D_2 by treating the message x_1 and AWGN n_1 as interference. We obtain the SINR when the near device D_1 decodes message x_2 as follows:

$$\gamma_{1-x_2}^{(HD)} = \frac{|h_1|^2\xi^{(HD)}\rho\alpha_2}{|h_1|^2\xi^{(HD)}\rho\alpha_1 + 1}, \quad (2)$$

where the Signal-to-Noise Ratio (SNR) $\rho = P/N_0$.

After detecting message x_2, the near device D_1 eliminates message x_2 from the received signal (1) and decodes its own message x_1 by treating AWGN n_1 as interference. We obtain the SINR when the near device D_1 decodes message x_1 as follows:

$$\gamma_{1-x_1}^{(HD)} = |h_1|^2\xi^{(HD)}\rho\alpha_1. \quad (3)$$

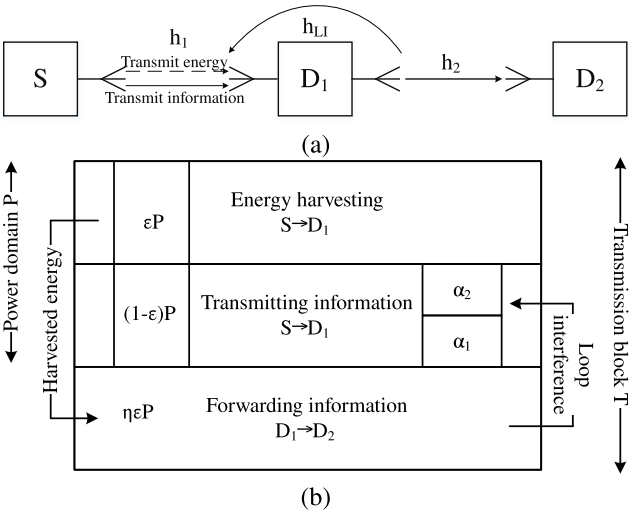

FIGURE 2. (a) An FD-IoT underlay cooperative NOMA network in combination with SWIPT; (b) PS diagram with FD relaying.

The instantaneous bit-rate threshold is reached when the near device D_1 decodes the messages x_i, as follows:

$$R_{1-x_i}^{(HD)} = \frac{1}{2}\log_2\left(1 + \gamma_{1-x_i}^{(HD)}\right), \quad (4)$$

where $i = \{2, 1\}$, respectively.

B. CONCEPT AND FORMULATION OF AN IoT UNDERLAY COOPERATIVE NOMA NETWORK WITH FD RELAYING

To reach ultra-low latency as the second aim of this study, we deployed the FD protocol at the near device D_1 to reduce the time delay at device D_2 (Figure 2a). D_1 is equipped with one antenna to receive the signal from source S and another to forward the signal to device D_2. The resulting transmission block is depicted in Figure 2b. It is important to note that only one time slot is available to finish a transmission block.

Figure 2b also illustrates EH and signal processing through the deployment of PS protocols shown in Figure1b. However, EH, information processing and information forwarding have three tiers. In tier 3, note the loop interference (LI) channel which is generated because D_1 adopts the FD protocol.

In an FD-IoT network model, the received signal at the near device D_1 from source S can be rewritten as follows:

$$y_1^{(FD)} = \underbrace{h_1\sqrt{\xi^{(FD)}P}\left(\sqrt{\alpha_1}x_1 + \sqrt{\alpha_2}x_2\right)}_{\text{Superimposed information}} + \underbrace{h_{LI}\eta\sqrt{\varepsilon^{(FD)}P}\tilde{x}}_{\text{Loop interference}} + \underbrace{n_1}_{\text{AWGN}}, \quad (5)$$

where PS factors $\varepsilon^{(FD)}$ and $\xi^{(FD)}$ are used for transmitting wireless energy and information, respectively, and $\xi^{(FD)} + \varepsilon^{(FD)} = 1$. Notice that PS factors $\varepsilon^{(FD)}$ and $\xi^{(FD)}$ in (5) are different comparing to the PS factors $\varepsilon^{(HD)}$ and $\xi^{(HD)}$ in (1). h_{LI} is also modeled as a Rayleigh fading channel with constrained $\sigma_{LI} = E\left\{|h_{LI}|^2\right\} = \varpi E\left\{|h_1|^2\right\}$ for $0 \leq \varpi \leq 1$, which refers to the LI impact factor. It is important to note

the LI in (5) relates to the EH at D_1 given by (56). The near device D_1 uses harvested energy from source S as transmit power to forward the signal to the far device D_2.

By applying SIC, the near device D_1 obtains the SINR when it decodes the message x_2 by treating the message x_1, LI channel h_{LI} and AWGN n_1 as interference as follows:

$$\gamma_{1-x_2}^{(FD)} = \frac{|h_1|^2 \xi^{(FD)} \rho \alpha_2}{|h_1|^2 \xi^{(FD)} \rho \alpha_1 + |h_{LI}|^2 \eta^2 \varepsilon^{(FD)} \rho + 1}. \quad (6)$$

After message x_2 is detected, it is eliminated from the received signal (5). The near device D_1 decodes its own message x_1 by treating the LI channel h_{LI} and AWGN n_1 as interference. The SINR is obtained as follows:

$$\gamma_{1-x_1}^{(FD)} = \frac{|h_1|^2 \xi^{(FD)} \rho \alpha_1}{|h_{LI}|^2 \eta^2 \varepsilon^{(FD)} \rho + 1}. \quad (7)$$

The instantaneous bit-rate threshold is reached at the near device D_1 in FD-IoT network model, as follows:

$$R_{1-x_i}^{(FD)} = \log_2 \left(1 + \gamma_{1-x_i}^{(FD)}\right). \quad (8)$$

where $i = \{2, 1\}$, respectively.

After message x_2 of the far device D_2 is decoded and eliminated, the near device D_1 retrieves message x_2 and forwards it to far device D_2 by adopting DF protocol.

The researchers have investigated forwarding protocols such as the DF protocol [10], AF with the FG protocol [21] and AF with the VG protocol [16]. The authors proved AF-VG protocol given the best performance [16]. Besides, the authors in study [52] deployed multiple antennas on all networking nodes and TAS protocol. The authors exploited the instantaneous AF factor maximization for AF-VG to optimize the system performance. However, this study chooses DF protocol because, on one hand, this protocol may approach responsive requirement to definitely ensure that device D_1 correctly receives the signal transmitted from source S and successfully decode the D_2's message x_2 before forwarding the message x_2 to far device D_2. On another hand, this study assumes device D_1 has enough energy for substantive operation. As a potential threat, device D_1 uses itself power for forwarding signal to device D_2 that may lead to out of power at device D_1. It means that AF protocol is impossible to be adopted at device D_1. Figures 1b and 2b illustrated that the near device D_1 used harvested energy as (56) to forward the signal to far device D_2. The received signal at the far device D_2 is therefore expressed as follows:

$$y_2^{(\varphi)} = h_1 h_2 \eta \sqrt{\varepsilon^{(\varphi)} P} x_2 + n_2, \quad (9)$$

where $\varphi = \{HD, FD\}$ and h_2 is the fading channel from the near device D_1 to the far device D_2. As with h_1, the fading channel h_2 is modeled according to Rayleigh distribution such that $h_2 = d_2^{-\omega}$, where d_2 is the distance $D_1 \to D_2$ and n_2 is the AWGN at device D_2 such that $n_2 \sim (0, N_0)$, with zero mean and variance N_0.

The far device D_2 implements SIC to decode its own message x_2 in the received signal (9) and obtains the SINR

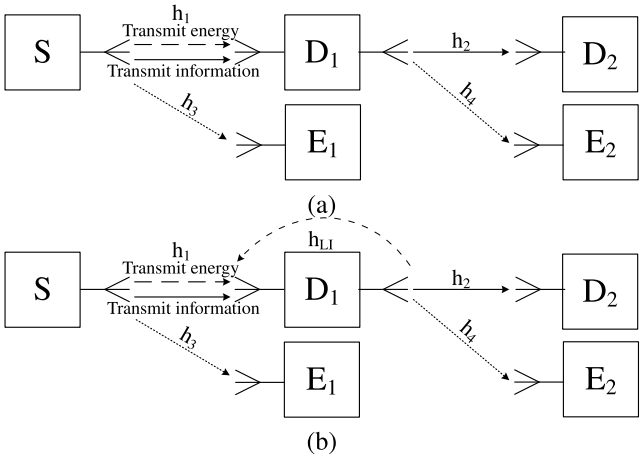

FIGURE 3. IoT networks with eavesdroppers.

when it decodes x_2 by treating AWGN n_2 as interference, as follows:

$$\gamma_{2-x_2}^{(\varphi)} = |h_1|^2 |h_2|^2 \eta^2 \varepsilon^{(\varphi)} \rho. \quad (10)$$

The instantaneous bit-rate threshold is reached when the far device D_2 decodes message x_2, as follows:

$$R_{2-x_2}^{(\varphi)} = \begin{cases} \frac{1}{2}\log_2 \left(1 + \gamma_{2-x_2}^{(\varphi)}\right), & \text{where } \varphi = HD, \\ \log_2 \left(1 + \gamma_{2-x_2}^{(\varphi)}\right), & \text{where } \varphi = FD. \end{cases} \quad (11)$$

C. CONCEPT AND FORMULATION OF AN IoT UNDERLAY COOPERATIVE NOMA NETWORKS WITH PLS

In this section, we assume that the IoT network contains eavesdroppers E_1 and E_2 (Figures 3a and 3b).

Note that the eavesdropper E_1 is allocated near D_1 or S, the system models (Figures 3a and 3b) would be similar to those described in featured studies [36] and [42]. The eavesdropper E_1 wants to eavesdrop device D_1. Device D_2 sends the SYN message to both the near device D_1 and eavesdropper E_1. In this case, D_1 and E_1 receive the SYN requirement of device D_2. However, eavesdropper E_1 is a passive device and unwell-known in the network. Hence, only device D_1 replies with an ACK message to device D_2. Device D_2 sends a FIN message to accept cooperation from device D_1. Device D_1 is implemented as a relay to assist device D_2. Because eavesdropper E_1 is near device D_1, it therefore receives the signal from S over the wiretapping channel h_3 as follows:

$$y_3^{(\varphi)} = h_3 \sqrt{\xi^{(\varphi)} P} \left(\sqrt{\alpha_1} x_1 + \sqrt{\alpha_2} x_2\right) + n_3, \quad (12)$$

where h_3 is the wiretapping channel, which is modeled as a Rayleigh fading channel with $h_3 = d_3^{-\omega}$, where d_3 is the distance from source S to eavesdropper E_1 and n_3 is the AWGN at eavesdropper E_1 such that $n_3 \sim (0, N_0)$, with zero mean and variance N_0.

The eavesdropper E_1 may implement SIC to decode the data symbols x_2 and x_1 and obtains the respective SINRs as follows:

$$\gamma_{3-x_2}^{(\varphi)} = \frac{|h_3|^2 \xi^{(\varphi)} \rho \alpha_2}{|h_3|^2 \xi^{(\varphi)} \rho \alpha_1 + 1}, \tag{13}$$

and

$$\gamma_{3-x_1}^{(\varphi)} = |h_3|^2 \xi^{(\varphi)} \rho \alpha_1. \tag{14}$$

The instantaneous bit-rate threshold is reached when the eavesdropper E_1 decodes the message x_i, where $i = \{2, 1\}$, as follows:

$$R_{3-x_i}^{(\varphi)} = \begin{cases} \frac{1}{2}\log_2\left(1 + \gamma_{3-x_i}^{(\varphi)}\right), & \text{where } \varphi = HD, \\ \log_2\left(1 + \gamma_{3-x_i}^{(\varphi)}\right), & \text{where } \varphi = FD. \end{cases} \tag{15}$$

The secrecy bit-rate threshold at the device D_1 is therefore given as follows:

$$\mathcal{R}_{1-x_i}^{(\varphi)} = \left[R_{1-x_i}^{(\varphi)} - R_{3-x_i}^{(\varphi)}\right]^+, \tag{16}$$

where $i = \{2, 1\}$.

The eavesdropper E_2 wants to eavesdrop device D_2. The device D_2 sends a SYN message to both the near device D_1 and eavesdropper E_2. In this case, D_1 and E_2 receive a SYN requirement for the device D_2. However, eavesdropper E_2 is a passive device and outside the cell network. Hence, only device D_1 replies with an ACK message to device D_2. Device D_2 sends a FIN message to accept cooperation with device D_1. Device D_1 is implemented as a relay to assist device D_2. Because the eavesdropper E_2 is near device D_2, it therefore receives the forwarding signal from device D_1 over the wiretapping channel h_4, as follows:

$$y_4^{(\varphi)} = h_1 h_4 \eta \sqrt{\varepsilon^{(\varphi)} P} x_2 + n_4, \tag{17}$$

where h_4 is the wiretapping channel, which is modeled as a Rayleigh fading channel with $h_4 = d_4^{-\omega}$, where d_4 is the distance from device D_1 to eavesdropper E_2 and n_4 is the AWGN at eavesdropper E_2 such that $n_4 \sim (0, N_0)$, with zero mean and variance N_0.

The system models (Figures 3a and 3b) resembles the system model in [43], where the eavesdropper is near the destination. However, the main aim in this study is to guarantee QoS at the far device and prove that the suitable PS factor may improve secrecy performance.

We assume that the eavesdropper E_2 is able to decode the data symbol x_2 when eavesdropper E_2 eavesdrops device D_2. Eavesdropper E_2 therefore obtains the respective SINR and instantaneous bit-rate threshold when it decodes the data symbol x_2, as follows:

$$\gamma_{4-x_2}^{(\varphi)} = |h_1|^2 |h_4|^2 \eta^2 \varepsilon^{(\varphi)} \rho, \tag{18}$$

and

$$R_{4-x_2}^{(\varphi)} = \begin{cases} \frac{1}{2}\log_2\left(1 + \gamma_{4-x_2}^{(\varphi)}\right), & \text{where } \varphi = HD, \\ \log_2\left(1 + \gamma_{4-x_2}^{(\varphi)}\right), & \text{where } \varphi = FD. \end{cases} \tag{19}$$

The secrecy bit-rate threshold at device D_2 is therefore given as follows:

$$\mathcal{R}_2^{(\varphi)} = \left[R_{2-x_2}^{(\varphi)} - R_{4-x_2}^{(\varphi)}\right]^+. \tag{20}$$

III. SYSTEM PERFORMANCE ANALYSIS

The PDF (f) and CDF (F) over Rayleigh distributions are expressed, respectively, as:

$$f_{|h_{(.)}|^2}(x) = \frac{1}{\sigma_{(.)}^2} \exp\left(-\frac{x}{\sigma_{(.)}^2}\right), \tag{21}$$

and

$$F_{|h_{(.)}|^2}(x) = 1 - \exp\left(-\frac{x}{\sigma_{(.)}^2}\right), \tag{22}$$

where x is a randomly independent variable such that $x \geq 0$ and $\sigma_{(.)}^2 = E\left\{|h_{(.)}|^2\right\}$.

A. OP PERFORMANCE

Theorem 1: The OP at near device D_1 in an HD/FD-IoT network model follows two cases:

- Either the instantaneous bit-rate threshold as given by (4) or (8), where $i = 2$, when the near device D_1 decodes message x_2, cannot reach the data rate threshold R_2 of device D_2, i.e. $R_{1-x_2}^{(\varphi)} < R_2$, where $\varphi = \{HD, FD\}$.
- Or the instantaneous bit-rate threshold as given by (4) or (8), where $i = 2$, when the near device D_1 decodes message x_2, reaches the data rate threshold R_2 of the far device D_2. However, the near device D_1 cannot decode its own message x_1, i.e. $R_{1-x_2}^{(\varphi)} \geq R_2$ and $R_{1-x_1}^{(\varphi)} < R_1$, where R_1 is the data rate threshold of device D_1.

The OP at the near device D_1 is expressed as:

$$OP_1^{(\varphi)} = \Pr\left\{R_{1-x_2}^{(\varphi)} < R_2\right\} + \Pr\left\{R_{1-x_2}^{(\varphi)} \geq R_2, R_{1-x_1}^{(\varphi)} < R_1\right\}. \tag{23}$$

By applying the PDF and CDF as given by (21) and (22), we obtain, in closed-form, the OP at the near device D_1 for an HD-IoT model, as follows:

$$OP_1^{(HD)} = 1 - \exp\left(-\frac{\gamma_2^{(HD)}}{\xi^{(HD)}\left(\alpha_2 - \alpha_1 \gamma_2^{(HD)}\right)\rho\sigma_1}\right) + \left[\exp\left(-\frac{\gamma_2^{(HD)}}{\xi^{(HD)}\left(\alpha_2 - \alpha_1 \gamma_2^{(HD)}\right)\rho\sigma_1}\right) - \exp\left(-\frac{\gamma_1^{(HD)}}{\xi^{(HD)}\alpha_1 \rho\sigma_1}\right)\right]^+, \tag{24}$$

where the SINR threshold is $\gamma_i^{(HD)} = 2^{2R_i} - 1$ for $i = \{2, 1\}$, respectively, and $\sigma_1 = E\left\{|h_1|^2\right\}$. From (24), we examine and then exploit three special cases. In the special first case, the OP at D_1 may refer to OP as $OP_1^{(HD)} = 1 - \exp\left(-\gamma_1^{(HD)} \Big/ \left(\xi^{(HD)}\alpha_1 \rho\sigma_1\right)\right)$, where

$R_2 < \frac{1}{2}\log_2\left(\frac{\alpha_2-\alpha_1}{\alpha_1}+1\right)$. And, in the second special case, the OP at D_1 may refer to OP as $OP_1^{(HD)} = 1 - \exp\left(-\gamma_2^{(HD)}\Big/\left(\xi^{(HD)}\left(\alpha_2-\alpha_1\gamma_2^{(HD)}\right)\rho\sigma_1\right)\right)$, where $R_2 \geq \frac{1}{2}\log_2\left(\frac{\alpha_2-\alpha_1}{\alpha_1}+1\right)$. In the third special case, OP at D_1 may $OP_1^{(HD)} \to 1$, where $R_2 \geq \frac{1}{2}\log_2\left(\frac{\alpha_2}{\alpha_1}+1\right)$.

By applying the PDF as given by (21), we obtain, in closed form, to the best of our knowledge, the novel closed-form of OP at the near device D_1 for an FD-IoT model, as follows:

$$\begin{aligned} OP_1^{(FD)} &= 1 - \frac{\xi^{(FD)}\left(\alpha_2-\alpha_1\gamma_2^{(FD)}\right)}{\xi^{(FD)}\left(\alpha_2-\alpha_1\gamma_2^{(FD)}\right)+\eta^2\varpi\varepsilon^{(FD)}\gamma_2^{(FD)}} \\ &\quad\times\exp\left(-\frac{\gamma_2^{(FD)}}{\xi^{(FD)}\left(\alpha_2-\alpha_1\gamma_2^{(FD)}\right)\rho\sigma_1}\right) \\ &\quad+\left[\frac{\xi^{(FD)}\left(\alpha_2-\alpha_1\gamma_2^{(FD)}\right)}{\xi^{(FD)}\left(\alpha_2-\alpha_1\gamma_2^{(FD)}\right)+\eta^2\varpi\varepsilon^{(FD)}\gamma_2^{(FD)}}\right. \\ &\quad\times\exp\left(-\frac{\gamma_1^{(FD)}}{\xi^{(FD)}\left(\alpha_2-\alpha_1\gamma_2^{(FD)}\right)\rho\sigma_1}\right) \\ &\quad\left.-\frac{\xi^{(FD)}\alpha_1}{\xi^{(FD)}\alpha_1+\eta^2\varpi\varepsilon^{(FD)}\gamma_1^{(FD)}}\exp\left(-\frac{\gamma_1^{(FD)}}{\xi^{(FD)}\alpha_1\rho\sigma_1}\right)\right]^+, \end{aligned} \tag{25}$$

where $\gamma_i^{(FD)} = 2^{R_i}-1$ for $i = \{2,1\}$. From (25), we examine and also exploit three special cases. In the first special case, the OP at device D_1 refers to $OP_1^{(FD)} = 1 - \frac{\xi^{(FD)}\alpha_1}{\xi^{(FD)}\alpha_1+\eta^2\varpi\varepsilon^{(FD)}\gamma_1^{(FD)}}\exp\left(-\frac{\gamma_1^{(FD)}}{\xi^{(FD)}\alpha_1\rho\sigma_1}\right)$, where $R_2 < \log_2\left(\frac{\alpha_2-\alpha_1}{\alpha_1}+1\right)$. In the second special case, the OP at device D_1 refers to $OP_1^{(FD)} = 1 - Q_3$, where $R_2 \geq \log_2\left(\frac{\alpha_2-\alpha_1}{\alpha_1}+1\right)$. In the third special case, the OP at device D_1 refers to $OP_1^{(FD)} = 1$, where $R_2 \geq \log_2\left(\frac{\alpha_2}{\alpha_1}+1\right)$.

Notice that OP performance at device D_1, where D_1 adopted FD mode and SNR $\rho \to \infty$, as given by (25) will reach the floor as follows:

$$\begin{aligned} FOP_1^{(FD)} &= 1 - \frac{\xi^{(FD)}\left(\alpha_2-\alpha_1\gamma_2^{(FD)}\right)}{\xi^{(FD)}\left(\alpha_2-\alpha_1\gamma_2^{(FD)}\right)+\eta^2\varpi\varepsilon^{(FD)}\gamma_2^{(FD)}} \\ &\quad+\left[\frac{\xi^{(FD)}\left(\alpha_2-\alpha_1\gamma_2^{(FD)}\right)}{\xi^{(FD)}\left(\alpha_2-\alpha_1\gamma_2^{(FD)}\right)+\eta^2\varpi\varepsilon^{(FD)}\gamma_2^{(FD)}}\right. \\ &\quad\left.-\frac{\xi^{(FD)}\alpha_1}{\xi^{(FD)}\alpha_1+\eta^2\varpi\varepsilon^{(FD)}\gamma_1^{(FD)}}\right]^+. \end{aligned} \tag{26}$$

From (24), notice that $OP_1^{(HD)}$ may tend to zero when SNR $\rho \to \infty$. However, $OP_1^{(FD)}$ as (25) may tend to $FOP_1^{(FD)}$ when $\rho \to \infty$.

See Appendix A for proof.

Lemma 1: Based on Theorem 1, it is challenging to investigate the OP at the device in closed-form, whereas massive devices joined the IoT network, for example, in [9], [10]. Functioning as a relay, device D_1 must decode the data symbols in a superimposed signal sequentially and forward the superimposed signal to the destination. We therefore propose a min-instantaneous bit-rate threshold framework to investigate OP performance at the devices. To illustrate, device D_1 receives the signal as given by (1) for HD scenario or (5) for FD scenario. By applying SIC, device D_1 obtains the SINR when it decodes the data symbols as given by (2) and (3) for HD scenario or (6) and (7) for FD scenario. As in previous major studies, the authors assumed that devices owned the same data rate thresholds for fairness as in [10], [11]. By applying min-rate framework, the OP event at device D_1 in this study may occur when the min-instantaneous bit-rate threshold cannot reach the data rate threshold $R = R_1 = R_2$. The min-rate OP at device D_1 is therefore expressed as follows:

$$\begin{aligned} MOP_1^{(\varphi)} &= \max\left\{\Pr\left\{R_{1-x_2}^{(\varphi)} < R_2\right\}, \Pr\left\{R_{1-x_1}^{(\varphi)} < R_1\right\}\right\}, \quad (27) \\ &= 1 - \Pr\left\{\min\left\{R_{1-x_2}^{(\varphi)}, R_{1-x_1}^{(\varphi)}\right\} \geq R\right\}, \quad (28) \end{aligned}$$

where $R_1 \neq R_2$ in (27) and $R_1 = R_2 = R$ in (28).

By observation of (28), only the minimum between the instantaneous bit-rate thresholds is applied for comparison to the device data threshold R. If the minimum between the instantaneous bit-rate thresholds achieves the device data threshold R, the maximum between the instantaneous bit-rate thresholds achieves the device data threshold R as a result. Therefore, the maximum between the instantaneous bit-rate thresholds need not be used to investigate the OP performance at device D_1. We may observe that equation (28) has a less complicated algorithm than equation (23). As a result, equation (28) requires less processing time to investigate the OP performance at device D_1.

By applying the PDF as given by (21), we obtain, in closed-form, the OP at device D_1 in HD and FD modes, respectively, as follows:

$$\begin{aligned} MOP_1^{(HD)} &= 1 - \exp\left(-\frac{\max\left\{\frac{\gamma_2^{(HD)}}{\left(\alpha_2-\alpha_1\gamma_2^{(HD)}\right)}, \frac{\gamma_1^{(HD)}}{\alpha_1}\right\}}{\xi^{(FD)}\rho\sigma_1}\right), \quad (29) \\ &= 1 - \exp\left(-\frac{\gamma^{(HD)}}{\xi^{(FD)}\rho\sigma_1\min\left\{\alpha_2-\alpha_1\gamma^{(HD)}, \alpha_1\right\}}\right), \quad (30) \end{aligned}$$

and

$$\begin{aligned} MOP_1^{(FD)} &= 1-\min\left\{\exp\left(-\frac{\gamma_2^{(FD)}}{\xi^{(FD)}\left(\alpha_2-\alpha_1\gamma_2^{(FD)}\right)\rho\sigma_1}\right)\right. \\ &\quad\times\frac{\xi^{(FD)}\left(\alpha_2-\alpha_1\gamma_2^{(FD)}\right)}{\xi^{(FD)}\left(\alpha_2-\alpha_1\gamma_2^{(FD)}\right)+\eta^2\varpi\varepsilon^{(FD)}\gamma_2^{(FD)}}, \\ &\quad\left.\exp\left(-\frac{\gamma_1^{(FD)}}{\xi^{(FD)}\alpha_1\rho\sigma_1}\right)\frac{\xi^{(FD)}\alpha_1}{\xi^{(FD)}\alpha_1+\eta^2\varpi\varepsilon\gamma_1^{(FD)}}\right\} \qquad (31) \\ &= 1-\exp\left(-\frac{\gamma^{(FD)}}{\xi^{(FD)}\rho\sigma_1\min\left\{\alpha_2-\alpha_1\gamma^{(FD)},\alpha_1\right\}}\right) \\ &\quad\times\frac{\xi^{(FD)}\min\left\{\alpha_2-\alpha_1\gamma^{(FD)},\alpha_1\right\}}{\xi^{(FD)}\min\left\{\alpha_2-\alpha_1\gamma^{(FD)},\alpha_1\right\}-\eta^2\varpi\varepsilon^{(FD)}\gamma^{(FD)}}, \qquad (32) \end{aligned}$$

where $R_1 \neq R_2$ in (29) and (31) and $R_1 = R_2 = R$ in (30) and (32), $\gamma^{(HD)} = 2^{2R}-1$, and $\gamma^{(FD)} = 2^R-1$.

From [29, Eq. (44)], the exponent function $\exp(-z) \approx 1-z$, where $z \to 0$ or SNR $\rho \to \infty$. Therefore, the OP performance at device D_1 in HD mode as given by (29) and (30) can be obtained in novel approximated forms, respectively, as follows:

$$\begin{aligned} AOP_1^{(HD)} &\approx \left\{\frac{\left\{\frac{\gamma_2^{(HD)}}{\left(\alpha_2-\alpha_1\gamma_2^{(HD)}\right)}\vee\frac{\gamma_1^{(HD)}}{\alpha_1}\right\}}{\xi^{(FD)}\rho\sigma_1}\wedge 1\right\}, \qquad (33) \\ &\approx 1-\left[1-\frac{\gamma^{(HD)}}{\xi^{(FD)}\rho\sigma_1\min\left\{\alpha_2-\alpha_1\gamma^{(HD)},\alpha_1\right\}}\right]^+, \qquad (34) \end{aligned}$$

such that $R_1 \neq R_2$ in (33) and $R_1 = R_2 = R$ in (34).

Similarly, we also obtain the approximate OP performance at the device D_2 in FD mode, as follows:

$$\begin{aligned} AOP_1^{(FD)} &\approx 1-\left\{\left(\left(1-\left\{1\wedge\frac{\gamma_2^{(FD)}}{\xi^{(FD)}\left(\alpha_2-\alpha_1\gamma_2^{(FD)}\right)\rho\sigma_1}\right\}\right)\right. \\ &\quad\times\frac{\xi^{(FD)}\left(\alpha_2-\alpha_1\gamma_2^{(FD)}\right)}{\xi^{(FD)}\left(\alpha_2-\alpha_1\gamma_2^{(FD)}\right)+\eta^2\varpi\varepsilon^{(FD)}\gamma_2^{(FD)}}\Bigg) \\ &\quad\wedge\left(\left(1-\left\{1\wedge\frac{\gamma_1^{(FD)}}{\xi^{(FD)}\alpha_1\rho\sigma_1}\right\}\right)\right. \\ &\quad\left.\left.\times\frac{\xi^{(FD)}\alpha_1}{\xi^{(FD)}\alpha_1+\eta^2\varpi\varepsilon^{(FD)}\gamma_1^{(FD)}}\right)\right\}, \qquad (35) \\ &\approx 1-\left(1-\left\{1\wedge\frac{\gamma^{(FD)}}{\xi^{(FD)}\rho\sigma_1\min\left\{\begin{matrix}\alpha_2-\alpha_1\gamma_2^{(FD)}\\ \alpha_1\end{matrix}\right\}}\right\}\right) \\ &\quad\times\frac{\xi^{(FD)}\min\left\{\alpha_2-\alpha_1\gamma^{(FD)},\alpha_1\right\}}{\xi^{(FD)}\min\left\{\begin{matrix}\alpha_2-\alpha_1\gamma_2^{(FD)}\\ \alpha_1\end{matrix}\right\}+\eta^2\varpi\varepsilon^{(FD)}\gamma^{(FD)}}, \qquad (36) \end{aligned}$$

such that $R_1 \neq R_2$ in (35) and $R_1 = R_2 = R$ in (36).

Notice that we exploit the floor of min-rate OP at device D_1, where D_1 adopted FD mode and SNR $\rho \to \infty$ as given by (31) and (32), as follows:

$$\begin{aligned} FOP_1^{(FD)} &= 1-\min\left\{\frac{\xi^{(FD)}\alpha_1}{\xi^{(FD)}\alpha_1+\eta^2\varpi\varepsilon^{(FD)}\gamma_1^{(FD)}},\right. \\ &\quad\left.\frac{\xi^{(FD)}\left(\alpha_2-\alpha_1\gamma_2^{(FD)}\right)}{\xi^{(FD)}\left(\alpha_2-\alpha_1\gamma_2^{(FD)}\right)+\eta^2\varpi\varepsilon^{(FD)}\gamma_2^{(FD)}}\right\} \qquad (37) \\ &= 1-\frac{\xi^{(FD)}\min\left\{\alpha_2-\alpha_1\gamma^{(FD)},\alpha_1\right\}}{\xi^{(FD)}\min\left\{\alpha_2-\alpha_1\gamma^{(FD)},\alpha_1\right\}-\eta^2\varpi\varepsilon^{(FD)}\gamma^{(FD)}}. \qquad (38) \end{aligned}$$

From (25), (31) for $R_1 \neq R_2$, (32) for $R_1 = R_2$, (35) for $R_1 \neq R_2$, (36) for $R_1 = R_2$, (37) for $R_1 \neq R_2$ and (38) for $R_1 = R_2$, we exploit $OP_1^{(FD)} = MOP_1^{(FD)} = AOP_1^{(FD)} = FOP_1^{(FD)}$ for SNR $\rho \to \infty$.

See Appendix B for proof.

Theorem 2: The OP at the far device D_2 with cooperation from the near device D_1 functioning in HD or FD mode has two cases:

- Either the near device D_1 cannot successfully decode message x_2 in the received signal (1) or (5). To illustrate, the achievable instantaneous bit-rate threshold as given by (4) or (8), where $i = 2$, cannot reach the data rate threshold R_2 of far device D_2, i.e. $R_{1-x_2}^{(\varphi)} < R_2$ for $\varphi = \{HD, FD\}$.
- Or the near device D_1 successfully decodes message x_2 of far device D_2 in the received signal (1) or (5). The near device D_1 retrieves message x_2 and forwards it to the far device D_2 by using the harvested energy as given by (56). However, the far device D_2 cannot successfully decode message x_2 in the received signal (9), i.e. $R_{1-x_2}^{(\varphi)} \geq R_2$ and $R_{2-x_2}^{(\varphi)} < R_2$.

The OP at the far device D_2 is expressed as follows:

$$\begin{aligned} OP_2^{(\varphi)} &= \Pr\left\{R_{1-x_2}^{(\varphi)} < R_2\right\} \\ &\quad+\Pr\left\{R_{1-x_2}^{(\varphi)} \geq R_2, R_{2-x_2}^{(\varphi)} < R_2\right\}. \qquad (39) \end{aligned}$$

By applying the PDF and CDF as (21) and (22), respectively, we obtain, in closed form, the OP at the far device D_2

in HD-IoT network model as follows:

$$OP_2^{(HD)} = 1 - \exp\left(-\frac{\gamma_2^{(HD)}}{\xi^{(HD)}\left(\alpha_2 - \alpha_1\gamma_2^{(HD)}\right)\rho\sigma_1}\right) + \left[\exp\left(-\frac{\gamma_2^{(HD)}}{\xi^{(HD)}\left(\alpha_2 - \alpha_1\gamma_2^{(HD)}\right)\rho\sigma_1}\right) - \frac{2B_1\left\{2\Big/\sqrt{\frac{\eta^2\varepsilon^{(HD)}\rho\sigma_1\sigma_2}{\gamma_2^{(HD)}}}\right\}}{\sqrt{\frac{\eta^2\varepsilon^{(HD)}\rho\sigma_1\sigma_2}{\gamma_2^{(HD)}}}}\right]^+, \quad (40)$$

where $\sigma_2 = E\left\{|h_2|^2\right\}$ and $B_1\{.\}$ is the second type of modified BesselK function [16].

Similarly, we obtain the OP at the far device D_2 for an FD-IoT network model as follows:

$$OP_2^{(FD)} = 1 - \exp\left(-\frac{\gamma_2^{(FD)}}{\xi^{(FD)}\left(\alpha_2 - \alpha_1\gamma_2^{(FD)}\right)\rho\sigma_1}\right) \times \frac{\xi^{(FD)}\left(\alpha_2 - \alpha_1\gamma_2^{(FD)}\right)}{\xi^{(FD)}\left(\alpha_2 - \alpha_1\gamma_2^{(FD)}\right) + \eta^2\varpi\varepsilon^{(FD)}\gamma_2^{(FD)}} + \left[\exp\left(-\frac{\gamma_2^{(FD)}}{\xi^{(FD)}\left(\alpha_2 - \alpha_1\gamma_2^{(FD)}\right)\rho\sigma_1}\right) \times \frac{\xi^{(FD)}\left(\alpha_2 - \alpha_1\gamma_2^{(FD)}\right)}{\xi^{(FD)}\left(\alpha_2 - \alpha_1\gamma_2^{(FD)}\right) + \eta^2\varpi\varepsilon^{(FD)}\gamma_2^{(FD)}} - \frac{2B_1\left\{2\Big/\sqrt{\frac{\eta^2\varepsilon^{(FD)}\rho\sigma_1\sigma_2}{\gamma_2^{(FD)}}}\right\}}{\sqrt{\frac{\eta^2\varepsilon^{(FD)}\rho\sigma_1\sigma_2}{\gamma_2^{(FD)}}}}\right]^+. \quad (41)$$

See Appendix C for proof.

Lemma 2: Based on Theorem 2, it is challenging to investigate the OP at the user in closed form, whereas multiple relaying nodes are deployed in IoT networks, for example, in [10]. The OP at device D_2 depends on the OP at device D_1. As in Lemma 1, we also deploy the min-instantaneous bit-rate threshold framework to investigate OP at the device D_2. To illustrate, device D_1 receives a signal as given by (1) for HD or (5) for FD. By applying SIC, device D_1 obtains the SINR when it decodes the data symbol x_2 as given by (2) for HD or (6) for FD. Device D_1 obtains instantaneous bit-rate as given by (4) for $\varphi = HD$ and $i = 2$ or (8) for $\varphi = FD$ and $i = 2$. Similarly, by applying SIC, the device D_2 decodes its own data symbol x_2 in received signal as given by (9) and obtains the SINR and instantaneous bit-rate threshold as given by (10) and (11), respectively. As a result, the OP event at device D_2 in this study may occur when the min-instantaneous bit-rate threshold cannot reach the data rate threshold R_2. The min-rate OP at device D_2 is therefore expressed as:

$$MOP_2^{(\varphi)} = \max\left\{O_{1-x_2}^{(\varphi)}, O_{2-x_2}^{(\varphi)}\right\} = 1 - \Pr\left\{\min\left\{R_{1-x_2}^{(\varphi)}, R_{2-x_2}^{(\varphi)}\right\} \geq R_2\right\}. \quad (42)$$

Min-rate OP at device D_2 in HD and FD scenarios are respectively obtained as follows:

$$MOP_2^{(\varphi)} = 1 - \left\{\exp\left(-\frac{\gamma_2^{(HD)}}{\xi^{(HD)}\left(\alpha_2 - \alpha_1\gamma_2^{(HD)}\right)\rho\sigma_1}\right) \wedge \frac{2B_1\left\{2\Big/\sqrt{\frac{\eta^2\varepsilon^{(HD)}\rho\sigma_1\sigma_2}{\gamma_2^{(HD)}}}\right\}}{\sqrt{\frac{\eta^2\varepsilon^{(FD)}\rho\sigma_1\sigma_2}{\gamma_2^{(HD)}}}}\right\}, \quad (43)$$

$$= 1 - \left\{\exp\left(-\frac{\gamma_2^{(FD)}}{\xi^{(FD)}\left(\alpha_2 - \alpha_1\gamma_2^{(FD)}\right)\rho\sigma_1}\right) \times \frac{\xi^{(FD)}\left(\alpha_2 - \alpha_1\gamma_2^{(FD)}\right)}{\xi^{(FD)}\left(\alpha_2 - \alpha_1\gamma_2^{(FD)}\right) + \eta^2\varpi\varepsilon^{(FD)}\gamma_2^{(FD)}} \wedge \frac{2B_1\left\{2\Big/\sqrt{\frac{\eta^2\varepsilon^{(FD)}\rho\sigma_1\sigma_2}{\gamma_2^{(FD)}}}\right\}}{\sqrt{\frac{\eta^2\varepsilon^{(FD)}\rho\sigma_1\sigma_2}{\gamma_2^{(FD)}}}}\right\}. \quad (44)$$

From expressions (43) and (44), the approximations of the min-rate OP performance at device D_2 are respectively expressed as:

$$AOP_2^{(HD)} \approx 1 - \left\{\left(1 - \left\{1 \wedge \frac{\gamma_2^{(HD)}}{\xi^{(HD)}\left(\alpha_2 - \alpha_1\gamma_2^{(HD)}\right)\rho\sigma_1}\right\}\right) \wedge \frac{2B_1\left\{2\Big/\sqrt{\frac{\eta^2\varepsilon^{(HD)}\rho\sigma_1\sigma_2}{\gamma_2^{(HD)}}}\right\}}{\sqrt{\frac{\eta^2\varepsilon^{(FD)}\rho\sigma_1\sigma_2}{\gamma_2^{(HD)}}}}\right\}, \quad (45)$$

and

$$AOP_2^{(FD)} \approx 1 - \left\{\left(\left(1 - \left\{1 \wedge \frac{\gamma_2^{(FD)}}{\xi^{(FD)}\left(\alpha_2 - \alpha_1\gamma_2^{(FD)}\right)\rho\sigma_1}\right\}\right) \times \frac{\xi^{(FD)}\left(\alpha_2 - \alpha_1\gamma_2^{(FD)}\right)}{\xi^{(FD)}\left(\alpha_2 - \alpha_1\gamma_2^{(FD)}\right) - \eta^2\varpi\varepsilon^{(FD)}\gamma_2^{(FD)}}\right) \wedge \frac{2B_1\left\{2\Big/\sqrt{\frac{\eta^2\varepsilon^{(FD)}\rho\sigma_1\sigma_2}{\gamma_2^{(FD)}}}\right\}}{\sqrt{\frac{\eta^2\varepsilon^{(FD)}\rho\sigma_1\sigma_2}{\gamma_2^{(FD)}}}}\right\}. \quad (46)$$

Let $W = 2B_1 \left\{2 \Big/ \sqrt{\frac{\eta^2 \varepsilon^{(FD)} \rho \sigma_1 \sigma_2}{\gamma_2^{(FD)}}}\right\} \Big/ \sqrt{\frac{\eta^2 \varepsilon^{(FD)} \rho \sigma_1 \sigma_2}{\gamma_2^{(FD)}}}$ and $V = 1 - Q_3$. The expressions W in (41) and (44) may tend to one while V may tend to the ceiling non-OP when SNR $\rho \to \infty$. As a result, we exploit the floor of OP $FOP_2^{(FD)}$ at device D_2 as follows:

$$FOP_2^{(FD)} = 1 - \frac{\xi^{(FD)} \left(\alpha_2 - \alpha_1 \gamma_2^{(FD)}\right)}{\xi^{(FD)} \left(\alpha_2 - \alpha_1 \gamma_2^{(FD)}\right) - \eta^2 \varpi \varepsilon^{(FD)} \gamma_2^{(FD)}}. \quad (47)$$

From (41), (44), (46) and (47), it is worth to notice that $OP_2^{(FD)} = MOP_2^{(FD)} = AOP_2^{(FD)} = FOP_2^{(FD)}$ for SNR $\rho \to \infty$.

B. SECRECY OP PERFORMANCE

In this section, we assume the presence of eavesdroppers E_1 nearby device D_1 to eavesdrop device D_1 and E_2 nearby device D_2 to eavesdrop device D_2 in the IoT network as shown in Figures 3a and 3b.

The secrecy OP at device D_1 follows two cases:

- On one hand, the secrecy instantaneous bit-rate threshold $\mathcal{R}_{1-x_2}^{(\varphi)}$ cannot reach bit-rate threshold R_2.
- On another hand, the secrecy instantaneous bit-rate threshold $\mathcal{R}_{1-x_2}^{(\varphi)}$ can reach bit-rate threshold R_2. However, The secrecy instantaneous bit-rate threshold $\mathcal{R}_{1-x_1}^{(\varphi)}$ cannot reach bit-rate threshold R_1.

In other word, the SOP performance at device D_1 is expressed as:

$$\begin{aligned} SOP_1^{(\varphi)} &= \Pr\left\{\left[R_{1-x_2}^{(\varphi)} - R_{3-x_2}^{(\varphi)}\right]^+ < R_2\right\} \\ &\quad + \Pr\left\{\left[R_{1-x_2}^{(\varphi)} - R_{3-x_2}^{(\varphi)}\right]^+ \geq R_2\,, \right. \\ &\quad \left. \left[R_{1-x_1}^{(\varphi)} - R_{3-x_1}^{(\varphi)}\right]^+ < R_1\right\} \\ &= 1 - \Pr\left\{\left[R_{1-x_2}^{(\varphi)} - R_{3-x_2}^{(\varphi)}\right]^+ \geq R_2\,, \right. \\ &\quad \left. \left[R_{1-x_1}^{(\varphi)} - R_{3-x_1}^{(\varphi)}\right]^+ \geq R_1\right\}. \end{aligned} \quad (48)$$

Theorem 3: It is challenge to solve (48). However, this study deploys a min-rate framework. Hence, the secrecy OP performance at device D_1 occurs when the minimum of the secrecy rates given by (16), where $i = \{2, 1\}$, cannot reach the data rate threshold R. The secrecy OP at device D_1 is therefore expressed as:

$$SOP_1^{(\varphi)} = \Pr\left\{\left[R_{1-x_1}^{(\varphi)} - R_{3-x_1}^{(\varphi)}\right]^+ \vee \left[R_{1-x_2}^{(\varphi)} - R_{3-x_2}^{(\varphi)}\right]^+ < R\right\}. \quad (49)$$

We obtain secrecy OP performance at device D_1, whereas D_1 functions in HD mode, as follows:

$$\begin{aligned} SOP_1^{(HD)} &= 1 - \left\{\frac{\alpha_2 \psi \pi}{2K \xi^{(HD)} \rho \sigma_3} \sum_{k=1}^{K} \left(\frac{\sqrt{1 - (2\Omega - 1)^2}}{(\alpha_2 - \alpha_1 \psi \Omega)^2} \right.\right. \\ &\quad \times \exp\left(-\frac{\psi \Omega}{\xi^{(HD)} (\alpha_2 - \alpha_1 \psi \Omega) \rho \sigma_3}\right) \\ &\quad \left.\left. \times \exp\left(-\frac{\tilde{\gamma}_2^{(HD)} \psi \Omega - 1}{\xi^{(HD)} \left(\alpha_2 - \alpha_1 \left(\tilde{\gamma}_2^{(HD)} \Omega - 1\right)\right) \rho \sigma_1}\right)\right) \right. \\ &\quad \left. \wedge \frac{\sigma_1}{\sigma_1 + \tilde{\gamma}_1^{(HD)} \sigma_3} \exp\left(-\frac{\gamma_1^{(HD)}}{\xi^{(HD)} \alpha_1 \rho \sigma_1}\right)\right\}, \end{aligned} \quad (50)$$

where K is the trade between accuracy and processing time, $\Omega = \frac{1}{2}\left(\cos\left(\frac{2k-1}{2K}\pi\right) + 1\right)$, and $\psi = \frac{1}{\alpha_1 \tilde{\gamma}_2^{(HD)}} - 1 < \frac{\alpha_2}{\alpha_1}$, and $\tilde{\gamma}_2^{(HD)} = \gamma_2^{(HD)} + 1$.

Secrecy OP performance at device D_1, whereas D_1 functions in FD mode, is expressed in closed-form as follows:

$$\begin{aligned} SOP_1^{(FD)} &= 1 - \left\{\left(\frac{\alpha_2 \delta \pi}{2K \xi^{(FD)} \rho \sigma_3 + \eta^2 \varepsilon^{(FD)} \varpi \tilde{\gamma}_2^{(FD)}} \right.\right. \\ &\quad \times \sum_{k=1}^{K} \left(\frac{\sqrt{1 - (2\Omega - 1)^2}}{(\alpha_2 - \alpha_1 \delta \Omega)^2 + \eta^2 \varepsilon^{(FD)} \varpi \tilde{\gamma}_2^{(FD)}} \right. \\ &\quad \times \exp\left(-\frac{\delta \Omega}{\xi^{(FD)} (\alpha_2 - \alpha_1 \delta \Omega) \rho \sigma_3}\right) \\ &\quad \left.\left.\left. \times \exp\left(-\frac{\tilde{\gamma}_2^{(FD)} \delta \Omega - 1}{\xi^{(FD)} \left(\alpha_2 - \alpha_1 \left(\tilde{\gamma}_2^{(FD)} \Omega - 1\right)\right) \rho \sigma_3}\right)\right)\right) \right. \\ &\quad \wedge - \frac{1}{\eta^2 \varepsilon^{(FD)} \varpi \rho \tilde{\gamma}_1^{(FD)} \sigma_3} \exp\left(-\frac{\gamma_1^{(FD)}}{\xi^{(FD)} \alpha_1 \rho \sigma_1}\right) \\ &\quad \times \left(\exp\left(-\frac{\left(\xi^{(FD)} \alpha_1 + \eta^2 \varepsilon^{(FD)} \varpi \gamma_1^{(FD)}\right) \chi}{\xi^{(FD)} \alpha_1 \eta^2 \varepsilon^{(FD)} \varpi \gamma_1^{(FD)} \rho \sigma_1 \sigma_3}\right)\right. \\ &\quad \times \left(\lim_{\Gamma \to \infty} \left(\sum_{\gamma=1}^{\Gamma} \frac{1}{\gamma} - \ln \Gamma\right) + \ln \frac{\chi}{\xi^{(FD)} \alpha_1 \rho \sigma_1 \sigma_3} \right. \\ &\quad \left.\left. - \ln \frac{\eta^2 \varepsilon^{(FD)} \varpi \tilde{\gamma}_1^{(FD)}}{\xi^{(FD)} \alpha_1 + \eta^2 \varepsilon^{(FD)} \varpi \gamma_1^{(FD)}}\right) \right. \\ &\quad \left.\left. - U\left\{1; 1; \frac{\left(\xi^{(FD)} \alpha_1 + \eta^2 \varepsilon^{(FD)} \varpi \gamma_1^{(FD)}\right) \chi}{\xi^{(FD)} \alpha_1 \eta^2 \varepsilon^{(FD)} \varpi \gamma_1^{(FD)} \rho \sigma_1 \sigma_3}\right\}\right)\right\}, \end{aligned} \quad (51)$$

where $\delta = \frac{1}{\tilde{\gamma}_2^{(FD)} (\alpha_1 + \eta^2 \varepsilon^{(FD)} \varpi)} - 1 < \frac{\alpha_2}{\alpha_1}$, $\chi = \sigma_1 + \tilde{\gamma}_1^{(FD)} \sigma_3$, and $U\{.;.;.\}$ is Kummer's confluent hypergeometric function.

See Appendix D for proof.

The secrecy OP events at far device D_2 occur in two cases:

- On one hand, the instantaneous bit-rate thresholds obtained at near device D_1 when it decodes data symbols x_2 as given by (5), where device D_1 functions in HD mode or (8) where device D_1 functions in FD mode, cannot reach the bit-rate threshold R_2 of device D_2.
- On another hand, the instantaneous secrecy bit-rate thresholds at near device D_1 when it decodes data symbol x_2 may reach the bit-rate threshold R_2. However, the instantaneous secrecy bit-rate threshold obtained at device D_2 when it decodes its own data symbol x_2 as given by (16) cannot reach the bit-rate threshold R_2.

Hence, the SOP at far device D_2 is expressed as:

$$\begin{aligned} &SOP_2^{(\varphi)} \\ &= \Pr\left\{R_{1-x_2}^{(\varphi)} < R_2\right\} \\ &\quad + \Pr\left\{R_{1-x_2}^{(\varphi)} \geq R_2\,,\, \left[R_{2-x_2}^{(\varphi)} - R_{4-x_2}^{(\varphi)}\right]^+ < R_2\right\} \\ &= 1 - \Pr\left\{R_{1-x_2}^{(\varphi)} \geq R_2\,,\, \left[R_{i-x_2}^{(\varphi)} - R_{(i+2)-x_2}^{(\varphi)}\right]^+ \geq R_2\right\}, \end{aligned} \tag{52}$$

where $i = \{2, 1\}$.

However, this study deploys a min-rate framework to obtain the OP at far device D_2, as given by Lemma 2.

Theorem 4: By applying a min-rate framework, the secrecy OP at far device D_2 in cooperation by near device D_1 functioning in HD or FD mode and without eavesdropper E_1 will occur if the minimum between $R_{1-x_2}^{(\varphi)}$ and $\mathcal{R}_2^{(\varphi)}$ cannot reach data rate threshold of device D_2.

In other work, the secrecy OP at device D_2 is expressed as:

$$\begin{aligned} &SOP_2^{(\varphi)} \\ &= 1 - \Pr\left\{\min\left\{R_{1-x_2}^{(\varphi)}, \left[R_{2-x_2}^{(\varphi)} - R_{4-x_2}^{(\varphi)}\right]^+\right\} \geq R\right\}. \end{aligned} \tag{53}$$

We obtain the secrecy OP at far device D_2 in closed-form as follows:

$$\begin{aligned} SOP_2^{(HD)} &= 1 - \exp\left(-\frac{\gamma_2^{(HD)}}{\xi^{(HD)}\left(\alpha_2 - \alpha_1\gamma_2^{(HD)}\right)\rho\sigma_1}\right) \\ &\quad + \left[\exp\left(-\frac{\gamma_2^{(HD)}}{\xi^{(HD)}\left(\alpha_2 - \alpha_1\gamma_2^{(HD)}\right)\rho\sigma_1}\right)\right. \\ &\quad \left. - \frac{2\sigma_2 B_1\left(2\sqrt{\frac{\eta^2\varepsilon^{(HD)}\rho\sigma_1\sigma_2}{\gamma_2^{(HD)}}}\right)}{\sqrt{\frac{\eta^2\varepsilon^{(HD)}\rho\sigma_1\sigma_2}{\gamma_2^{(HD)}}}\left(\sigma_2 + \sigma_4 + \gamma_2^{(HD)}\sigma_4\right)}\right]^+ \end{aligned} \tag{54}$$

and

$$\begin{aligned} SOP_2^{(FD)} &= 1 - \exp\left(-\frac{\gamma_2^{(FD)}}{\xi^{(FD)}\left(\alpha_2 - \alpha_1\gamma_2^{(FD)}\right)\rho\sigma_1}\right) \\ &\quad \times \frac{\xi^{(FD)}\left(\alpha_2 - \alpha_1\gamma_2^{(FD)}\right)}{\xi^{(FD)}\left(\alpha_2 - \alpha_1\gamma_2^{(FD)}\right) + \eta^2\varpi\varepsilon^{(FD)}\gamma_2^{(FD)}} \\ &\quad + \left[\exp\left(-\frac{\gamma_2^{(FD)}}{\xi^{(FD)}\left(\alpha_2 - \alpha_1\gamma_2^{(FD)}\right)\rho\sigma_1}\right)\right. \\ &\quad \times \frac{\xi^{(FD)}\left(\alpha_2 - \alpha_1\gamma_2^{(FD)}\right)}{\xi^{(FD)}\left(\alpha_2 - \alpha_1\gamma_2^{(FD)}\right) + \eta^2\varpi\varepsilon^{(FD)}\gamma_2^{(FD)}} \\ &\quad \left. - \frac{2\sigma_2 B_1\left(2\sqrt{\frac{\eta^2\varepsilon^{(FD)}\rho\sigma_1\sigma_2}{\gamma_2^{(FD)}}}\right)}{\sqrt{\frac{\eta^2\varepsilon^{(FD)}\rho\sigma_1\sigma_2}{\gamma_2^{(FD)}}}\left(\sigma_2 + \sigma_4 + \gamma_2^{(FD)}\sigma_4\right)}\right]^+. \end{aligned} \tag{55}$$

See Appendix E for proof.

Note that we analyzed the secrecy OP at device D_2 as (54) and (55) with only eavesdropper E_2 without consideration the impact from eavesdropper E_1. However, in practical IoT networks, eavesdroppers may be allocated anywhere in the networking coverage. Here, we assume there are multiple eavesdroppers. The eavesdropper E_1 is allocated near by device D_1. And, the eavesdropper E_2 is allocated near by device D_2. From (52). The secrecy OP at device D_2 in HD/FD IoT networks with multiple eavesdroppers E_1 and E_2 may be rewritten by $SOP_2^{(\varphi)} = 1 - \Pr\left\{R_{1-x_2}^{(\varphi)} < R\right\} + \Pr\left\{R_{1-x_2}^{(\varphi)} \geq R, R_2^{(\varphi)} < R\right\}$. Finally, we obtain the secrecy OP at device D_2 in HD and FD scenarios with multiple eavesdroppers as $SOP_2^{(HD)} = 1 - Q_8 + \left[Q_8 - Q_{11}^{(HD)}\right]^+$ and $SOP_2^{(FD)} = 1 - Q_{10} + \left[Q_{10} - Q_{11}^{(FD)}\right]^+$. It is not necessary to re-present expressions Q_8, Q_{10} and $Q_{11}^{(\varphi)}$ since they were given by (91), (94) and (96), respectively.

C. TWO-STAGE POWER RESOURCE ALLOCATION EXPLOITED TO ENHANCE SYSTEM PERFORMANCE

The first-stage is to deliver the PS factor. In [28], [29], [48], the authors investigated network models with a fixed PS factor, i.e. $\varepsilon = 0.4$. However, we consider how the PS factor affects system performance. Through observations of (1), (5) and (9), we can exploit two interesting cases. The first SWIPT case contains $\varepsilon = 0$. All power resources P at source S are only used to transmit the signals to the near device D_1. In this case, the near device D_1 receives the signal as given by (1) or (5) in the best received signal, but leads to the EH at the near device D_1 given by (56) tending to zero. Therefore, the near device D_1 has no power resources to forward signals. As a results, the OP at the far device D_2 always tends to one absolutely. The second SWIPT case has $\varepsilon = 1$. All power domain P at source S are only used to transmit wireless power for EH at the near device D_1. As a result, the OP performances at devices D_1 and D_2 always tend to one absolutely.

From (1) or (5), the EH at the near device D_1 is modelled by linear model [33] and expressed as follows:

$$EH^{(\varphi)} = \eta h_1 \sqrt{\varepsilon^{(\varphi)} P}, \tag{56}$$

where η is the collection factor such that $0 \leq \eta \leq 1$ [38]. We assume that the EH is not affected by the limitations of electronic circuitry and battery capacity ($\eta = 1$) as given in [31], [38]. In this linear EH model, the total EH at the device D_1 is linearly and directly relative to the received RF wireless power transmission. Therefore, it is expected that the linear EH model is accurate for the specific scenario when the received RF-EH at device D_1 is constant. In the study [34], the authors proposed a parameter for a non-linear EH model which is based on the variable of the RF-EH transformation efficiency for different input power levels [34, Eq. (4)]. It is worth highlighting why we selected the PS protocol and how our PS diagrams differs from the diagrams in the major studies [36], [48]. Although based on multi-relays, the system models in [36, Figure 1] and [48, Figures 1a] served only one destination. The system model in this study (Figures 1a, 2a) is understood as serving multi-devices. If we deploy a TS transmission time block structure [36, Figure 2] or [48, Figures 1b and 3b], it may lead to increased delay times in devices that need to be served simultaneously. The three-layers PS diagram (Figure 1b) requires two time slots to finish a transmission block. The first time slot is to adopt SWIPT from source S to device D_1. The top layer in Figure 1b is used for source S transmitting energy and the second layer is used for source S transmitting information to the device D_1. Devices need to be served simultaneously to reduce latency. Therefore, information of devices is superimposed by sharing different PA factors, where $\alpha_2 > \alpha_1$, $\left(1-\varepsilon^{(\varphi)}\right)\alpha_2 P + \left(1-\varepsilon^{(\varphi)}\right)\alpha_1 P = \left(1-\varepsilon^{(\varphi)}\right)P$, and $\left(1-\varepsilon^{(\varphi)}\right)P + \varepsilon^{(\varphi)}P = P$. Finally, as shown in the bottom layer in Figure 1b, the signal from device D_1 is forwarded to device D_2 after harvesting energy using the DF protocol.

Proposition 1: We constrain the SINR when the near device D_1 decodes message x_1 as given by (3) and the SINR when the far device D_2 decodes message x_2 as given by (10), approximately as follows:

$$\gamma_{1-x_1}^{(HD)} = \gamma_{2-x_2}^{(HD)}, \tag{57}$$

In the previous studies [21]–[23], the authors investigated cooperative NOMA networks which adopt the AF protocol at the relay. Two AF techniques can be used: AF with variable gain and AF with fixed gain. The amplify factors with variable gain have instantaneous CSI $|h|^2$. The amplify factors with fixed gain have expected channel gains $E\left\{|h|^2\right\}$ given by [21, Eq. (7)], [22, Eq. (9a)] and [23, Eq. (7)]. Note that the present work assumes a source fully owned by CSI. Therefore, we substituted the expected channel gain σ_1 and σ_2 into (57). We determined the PS factor $\varepsilon^{(HD)}$ for expressions (3) and (10) equally. By substituting the expected channel gains $\sigma_1 = E\left\{|h_1|^2\right\}$ and $\sigma_2 = E\left\{|h_2|^2\right\}$ into (57), we obtained the PS factor $\varepsilon^{(HD)}$ for an HD scenario under the constraints given by (57), as follows:

$$\varepsilon^{(HD)} = \frac{\alpha_1}{\sigma_2 + \alpha_1}. \tag{58}$$

We take advantage of the fact that $\varepsilon^{(HD)}$ is always greater than half and will tend to one if device D_2 is far away from D_1, i.e. $\varepsilon^{(HD)} > 0.5$ and $\varepsilon^{(HD)} \to 1$, whereas $\sigma_2 \to 0$. By substituting (58) into (1), we obtain the received signal at the device D_1, which adopts the HD protocol. To reach ultra-low latency, this study designed PS framework as shown Figure 2b. However, when we substitute (58) into (5), we always obtain $y_1^{(FD)} < y_1^{(HD)}$ because of the effect of LI. Therefore, we constrain the PS factor so that $0.5 \leq \varepsilon^{(FD)} \leq \varepsilon^{(HD)} < 1$. We therefore propose the PS factor, whereas D_1 adopts the FD protocol, as follows:

$$\begin{aligned} \mathcal{A} &\leftarrow int\left\{\sigma_2/\sigma_1\right\}, \\ \varepsilon^{(FD)} &\leftarrow \varepsilon^{(HD)}, \\ \underset{l\to\mathcal{A}}{Loop} &\left\{\varepsilon^{(FD)} \leftarrow \frac{l\varepsilon^{(FD)} + 0.5}{l+1}\right\}, \end{aligned} \tag{59}$$

where the *int* {.} function returns an integer value and $\mathcal{A}$ is the adjusted factor. It is important to note that the adjusted factor $\mathcal{A}$ is the fraction of expected channel gain σ_2 of the expected channel gain σ_1. To illustrate, this means that the distance $D_1 \to D_2$ is less than the distance $S \to D_1$ and the PS factor for FD scenario is significantly reduced, i.e. as the distances $d_2 \ll d_1$, as a result, $\sigma_2 \gg \sigma_1$ and the PS factor $\varepsilon^{(FD)}$ will be adjusted tending to half. Beside, if distance $D_1 \to D_2$ is greater than the distance $S \to D_1$, as a result, $d_2 > d_1$ and $\sigma_2 < \sigma_1$, the PS factor $\varepsilon^{(FD)}$ will be adjusted tending to $\varepsilon^{(HD)}$.

Proposition 2: In previous studies, the authors applied fixing PA factors [21], [28], [32]. In other studies, the authors adopted adaptive PA factors for multiple access based on the number of devices [9] or expected channel gain and the sum of the expected channel gain ratio [16]. In the second-stage of power resource allocation, the present study proposes adaptive PA factors for multiple access IoT networks based on the density distance of the data symbol propagated from the source to the destination. Therefore, the data symbol of the farthest device, which was propagated with the farthest distance and path-loss exponent, is allocated the largest PA factor, as follows:

$$\alpha_1 = \frac{d_1^{\omega}}{d_1^{\omega} + (d_1 + d_2)^{\omega}}, \tag{60}$$

and

$$\alpha_2 = \frac{(d_1 + d_2)^{\omega}}{d_1^{\omega} + (d_1 + d_2)^{\omega}}. \tag{61}$$

We propose Algorithm 1 for two-stages power resource allocation.

To confirm the theoretical results, we propose Monte Carlo simulations as Algorithm 2 to examine the OP performance and Algorithm 3 to examine the secrecy OP performance at the devices.

Algorithm 1 Two-Stages Power Resource Allocation

Input: Initialize the parameters as distances $d_1 = S \to D_1$ and $d_2 = D_1 \to D_2$, path-loss exponent ω, calculate expected channel gains $\sigma_1 = d_1^{-\omega}$ and $\sigma_2 = d_2^{-\omega}$

Output: PA factors and PS factors.

Calculate $\alpha_1 = \frac{d_1{}^{\omega}}{d_1{}^{\omega}+(d_1+d_2)^{\omega}}$;
Calculate $\alpha_2 = \frac{(d_1+d_2)^{\omega}}{d_1{}^{\omega}+(d_1+d_2)^{\omega}}$ or $1-\alpha_1$;
Calculate $\varepsilon^{(HD)} = \alpha_1 \big/ (\sigma_2 + \alpha_1)$;
$\mathcal{A} = int\left\{\sigma_2 \big/ \sigma_1\right\}$;
Initialize $\varepsilon^{(FD)} = \varepsilon^{(HD)}$;
for $l = 1$ to $\mathcal{A}$ **do**
  $\varepsilon^{(FD)} = \frac{l\varepsilon^{(FD)}+0.5}{l+1}$
end for
return $\alpha_1, \alpha_2, \varepsilon^{(HD)}, \varepsilon^{(FD)}$;

Lei *et al.* [40, Eq. (17)] obtained the OP performance of a two-device (2-D) downlink NOMA system. Generally, the OP system performance of 2-D in an HD/FD-IoT model is the mean of the OP performance at the devices. However, This study valuate the OP performance of a IoT system based on the worst OP performance of a device among OP performances of the devices as follows:

$$\mathcal{O}_{sys}^{(\varphi)} = \max\left\{\mathcal{O}_1^{(\varphi)}, \mathcal{O}_2^{(\varphi)}\right\}, \tag{62}$$

where $\mathcal{O}_i^{(\varphi)} = \left\{OP_i^{(\varphi)}, MOP_i^{(\varphi)}, AOP_i^{(\varphi)}\right\}$ for $i = \{2, 1\}$.

D. SYSTEM THROUGHPUT PERFORMANCE

From the OP results obtained at the near device D_1 and the far device D_2, we obtain the system throughput performance of the 2-D system as follows:

$$T^{(\varphi)} = \left(1 - \mathcal{O}_1^{(\varphi)}\right) R_1 + \left(1 - \mathcal{O}_2^{(\varphi)}\right) R_2. \tag{63}$$

E. QoS FAIRNESS

In this subsection, as regarding to the third aim, we investigate Jain's fairness index based on the reachable throughput at the devices as follows:

$$J^{(\varphi)} = \frac{\left(\mathcal{O}_1^{(\varphi)} + \mathcal{O}_2{}^{(\varphi)}\right)^2}{2\left(\left(\mathcal{O}_1^{(\varphi)}\right)^2 + \left(\mathcal{O}_2^{(\varphi)}\right)^2\right)}, \tag{64}$$

where Jain's fairness index $\mathcal{J}^{(\varphi)} \to 1$ and the devices are served with the same QoS of OP performance. However, whereas Jain's fairness index $J^{(\varphi)} \to 0$, it indicates that the devices are not served with the fairness QoS of OP performance. Therefore, we propose a sum of the cumulative flux deviation of devices' throughput from the mean flux throughput achieved at all devices, as follows:

$$\mathcal{T}^{(\varphi)} = \sum_{n=1}^{\mathcal{N}} \left| \left(1 - \mathcal{O}_n^{(\varphi)}\right) R_n - \frac{1}{\mathcal{N}} \sum\nolimits_{j=1}^{\mathcal{N}} \left(1 - \mathcal{O}_j^{(\varphi)}\right) R_j \right|, \tag{65}$$

where $\mathcal{N}$ is the number of networked IoT devices.

Algorithm 2 OP and Min-Rate OP Simulations

Input: Initialize the parameters as predefined data rates $R = R_1 = R_2$ bps/Hz, SNRs ρ in dB, expected channel gains $\sigma_1, \sigma_2, \sigma_{LI}$ with contributing LI factor ϖ, and randomly generate $1e6$ samples over each channel h_1, h_2 or h_{LI}. PA and PS factors are given by Algorithm 1.

Output: OP and min-rate OP simulation results at the devices.

Calculate $1e6$ SINRs $\gamma_{n-x_i}^{(\varphi)}$, where $n = \{1, 2\}$, $i = \{2, 1\}$, and $\varphi = \{HD, FD\}$, at devices given by (2), (3), (6), (7) or (10) at SNR ρ in the SNR range;
Calculate $1e6$ instantaneous data rate $R_{n-x_i}^{(\varphi)}$, where n is a device in a number of devices, i is a data symbol in a number of data symbols, and $\varphi = \{HD, FD\}$, at devices given by (4), (8) or (11);
Initialize $Count_n^{(\varphi)} = 0$ and $MCount_n^{(\varphi)} = 0$, where $n = \{1, 2\}$, $i = \{2, 1\}$ and $\varphi = \{HD, FD\}$ at a SNR ρ in the SNR range;
$LOOP = 1e6$;
for $i = 1$ to $LOOP$ **do**
  // Count successful rate at D_1
  if $\left(R_{1-x_2}^{(\varphi)} \geq R_2 \& R_{1-x_1}^{(\varphi)} \geq R_1\right)$ **then**
    $Count_{1-x_2}^{(\varphi)} \leftarrow Count_{1-x_2}^{(\varphi)} + 1$;
  end if
  // Count successful rate at D_2
  if $\left(R_{1-x_2}^{(\varphi)} \geq R_2 \& R_{2-x_2}^{(\varphi)} \geq R_2\right)$ **then**
    $Count_{2-x_2}^{(\varphi)} \leftarrow Count_{2-x_2}^{(\varphi)} + 1$;
  end if
  // Count successful min-rate at D_1
  if $\left(\min\left\{R_{1-x_1}^{(\varphi)}, R_{1-x_2}^{(\varphi)}\right\} \geq R\right)$ **then**
    $MCount_1^{(\varphi)} \leftarrow MCount_1^{(\varphi)} + 1$;
  end if
  // Count successful min-rate at D_2
  if $\left(\min\left\{R_{1-x_2}^{(\varphi)}, R_{2-x_2}^{(\varphi)}\right\} \geq R\right)$ **then**
    $MCount_2^{(\varphi)} \leftarrow MCount_2^{(\varphi)} + 1$;
  end if
end for
return
$OP_1^{(\varphi)} \leftarrow 1 - \frac{Count_1^{(\varphi)}}{LOOP}$;
$OP_2^{(\varphi)} \leftarrow 1 - \frac{Count_2^{(\varphi)}}{LOOP}$;
$MOP_1^{(\varphi)} \leftarrow 1 - \frac{MCount_1^{(\varphi)}}{LOOP}$;
$MOP_2^{(\varphi)} \leftarrow 1 - \frac{MCount_2^{(\varphi)}}{LOOP}$;

IV. NUMERICAL RESULTS AND DISCUSSIONS

The results presented in this section are true and accurate to the best of our knowledge, without any duplication from previous studies. In this study, we investigate the IoT network in Figures 1, 2 and 3, with HD-IoT and FD-IoT networks, respectively. The distances $S \to D_1$ denoted d_1, $S \to E_1$ denoted d_3, $D_1 \to D_2$ denoted d_2, and $D_1 \to E_2$ denoted d_4 are $d_1 = d_3 = 10$ m and $d_2 = d_4 = 2$ m. The path-loss

Algorithm 3 Secrecy OP and Min-Rate Secrecy OP Simulations

Input: Initialize the parameters as expected channel gains σ_3, σ_4, randomly generate $1e6$ samples on each channel h_3, h_4 distributed by Rayleigh distributions and the variables given by Algorithms 1 and 2.

Output: Secrecy OP and min-rate secrecy OP at the devices.

Calculate $1e6$ SINRs $\gamma_{m-x_i}^{(\varphi)}$, where m is a device or an eavesdropper with $m = \{1, 2, 3, 4\}$, i is a data symbol, where $i = \{2, 1\}$ and $\varphi = \{HD, FD\}$, at the devices, given by (2), (3), (6), (7), (10), (13), (14) and (18) at a SNR ρ in the SNR range;
Calculate $1e6$ instantaneous data rate $R_{m-x_i}^{(\varphi)}$ at devices as (4), (8) or (11);
Initialize $Count_{m-x_i}^{(\varphi)} = 0$;
$LOOP = 1e6$;
for $i = 1$ to $LOOP$ **do**
  // Count successful secrecy rate at D_1
  if $\left(\max\left\{R_{1-x_1}^{(\varphi)} - R_{3-x_1}^{(\varphi)}, 0\right\} \geq R_1\right)$ **then**
    $SCount_{1-x_1}^{(\varphi)} \leftarrow SCount_{1-x_1}^{(\varphi)} + 1$;
  end if
  if $\left(\max\left\{R_{1-x_2}^{(\varphi)} - R_{3-x_2}^{(\varphi)}, 0\right\} \geq R_2\right)$ **then**
    $SCount_{1-x_2}^{(\varphi)} \leftarrow SCount_{1-x_2}^{(\varphi)} + 1$;
  end if
  // Count successful secrecy rate at D_2
  if $\left(\max\left\{R_{2-x_2}^{(\varphi)} - R_{4-x_2}^{(\varphi)}, 0\right\} \geq R_2\right)$ **then**
    $SCount_{2-x_2}^{(\varphi)} \leftarrow SCount_{2-x_2}^{(\varphi)} + 1$;
  end if
end for
return

$$SOP_1^{(\varphi)} \leftarrow 1 - \frac{SCount_{1-x_2}^{(\varphi)}}{LOOP} \times \frac{SCount_{1-x_1}^{(\varphi)}}{LOOP};$$

$$SOP_2^{(\varphi)} \leftarrow 1 - \frac{SCount_{1-x_2}^{(\varphi)}}{LOOP} \times \frac{SCount_{2-x_2}^{(\varphi)}}{LOOP};$$

$$\text{Min-rate } SOP_1^{(\varphi)} \leftarrow 1 - \frac{SCount_{1-x_2}^{(\varphi)}}{LOOP} \wedge \frac{SCount_{1-x_1}^{(\varphi)}}{LOOP};$$

$$\text{Min-rate } SOP_2^{(\varphi)} \leftarrow 1 - \frac{SCount_{1-x_2}^{(\varphi)}}{LOOP} \wedge \frac{SCount_{2-x_2}^{(\varphi)}}{LOOP};$$

exponent factor is an indoor environment $\omega = 4$. The expected channel gains over Rayleigh distributions from source S to the near device D_1 and eavesdropper E_1 are $\sigma_1 = \sigma_3 = 0.0004$, and $\sigma_2 = \sigma_4 = 0.0625$ from device D_1 to device D_2 and eavesdropper E_2. LI impact factor $\varpi = 0.01$ and SNRs $\rho = \{10, \ldots, 40\}$ dB. The energy is fully harvested without the effect of limitations in the energy collection circuitry and battery capacity, and thus, for simplicity, $\eta = 1$ [38]. The PA factors for the near device D_1 and far device D_2, given by (60) and (61), respectively, are $\alpha_1 = 0.3254$ and $\alpha_2 = 0.6746$. The devices D_1 and D_2 require the same data rate threshold such that $R_1 = R_2 = 0.1$ bps/Hz.

We investigated three SWIPT cases:

- The first SWIPT case has a fixed PS factor $\varepsilon = 0.4$, i.e. 40% of the power domain is harvested at the near device D_1.
- The second SWIPT case has a PS factor $\varepsilon^{(HD)} = 0.8389$, given by (58). This means that 83.89% of the power domain P is used for transmit energy to the near device D_1 for EH.
- The third SWIPT case has PS factor $\varepsilon^{(FD)} = 0.5005$, given by (59). This means that 50.05% of the power domain P is used for transmit energy to the near device D_1 for EH.

Figure 4 depicts the work of this study briefly.

TABLE 1. Table of parameters.

Number of devices	2
Number of eavesdropper	2
Distances $d_1 = d_3$	$10\ m$
Distances $d_2 = d_4$	$2\ m$
Path-loss exponent ω	4
Channel gains $\sigma_1 = \sigma_3$	0.0004
Channel gains $\sigma_2 = \sigma_4$	0.0625
LI coefficient ϖ	0.01
Bit-rate thresholds $R_1 = R_2$	$0.1\ bps/Hz$
Collect factor η	1
Fixed PS factor ε	0.4
PS factor for HD scenario $\varepsilon^{(HD)}$	0.8389
PS factor for FD scenario $\varepsilon^{(FD)}$	0.5005
SNRs ρ	$\{10, \ldots, 40\}$ dB

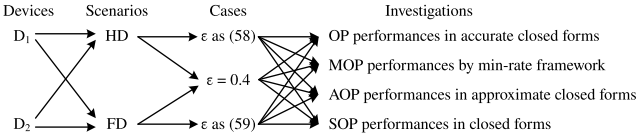

FIGURE 4. Scheme of the work in this study.

In this study, we use various indicators and lines to plot the analysis (Ana) results and Monte Carlo simulation (Sim) results.

A. OP PERFORMANCE

1) EFFECT OF THE PS FACTOR ON OP PERFORMANCE

The first aim of this study was to investigate the effect of the PS factor ε on system performance. Figures 5a and 5b depict OP performances at devices D_1 and D_2 with solid and dashed grids, respectively, where D_1 adopted either the HD or FD mode. There are two special cases of PS factors: $\varepsilon^{(\varphi)} = 0$ and $\varepsilon^{(\varphi)} = 1$. Where $\varepsilon^{(\varphi)} = 0$, the received signals at device D_1 given by (1) and (5) reached maximum volume, which indicates the best OP performance at D_1. However, the OP performance obtained at device D_2 always tended to one since the EH given by (56) at device D_1 tended to zero. As a result, device D_1 had no power to forward the signal to device D_2. Where $\varepsilon^{(\varphi)} = 1$, the received signals given by (1) and (5) reached minimum volume, and EH given by (56) at device D_1 reached maximum volume. Therefore, no information was available to forward to D_2. As a result, both devices D_1 and D_2 always achieved OP performance that tended to one at all SNR ρ. We can observe that the OP performance at the devices was affected by the PS factors. The main aim of this

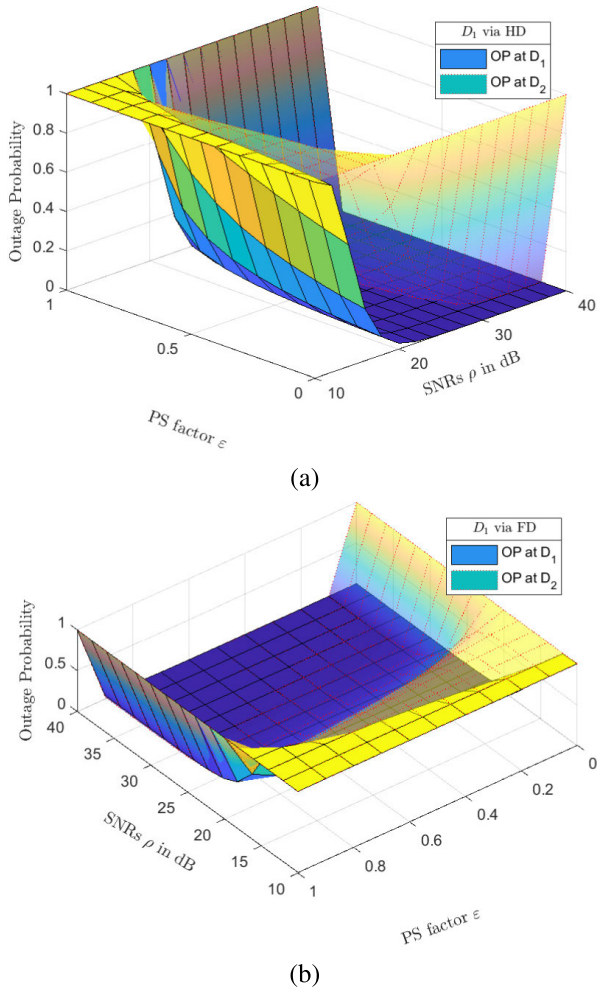

FIGURE 5. Investigations of the impact of PS factors on the OP performance of the devices: (a) D_1 adopts HD mode; (b) D_1 adopts FD mode.

study was to exploit suitable PS factors to guarantee QoS fairness at the devices.

2) OP PERFORMANCE AT THE DEVICES IN THE HD-IoT NETWORK MODEL

In the HD scenario, we investigated OP performances at devices D_1 and D_2 (Figures 6a and 6b) for two PS cases: a fixed PS factor $\varepsilon = 0.4$ as in [29] and a PS factor $\varepsilon^{(HD)}$ given by (58). We can observe in Figure 6a that the OP performance at device D_1 with fixed PS factor $\varepsilon = 0.4$ was better than the OP performance with PS factor $\varepsilon^{(HD)} = 0.8389$ given by (58) since the received signal $y_1^{(HD,\varepsilon=0.4)}$ was better than $y_1^{(HD,\varepsilon=0.8389)}$. However, it is important to observe in Figure 6b that the OP performance at device D_2 with PS factor $\varepsilon = 0.8389$ was better than the OP performance with fixed PS factor $\varepsilon = 0.4$ since device D_1 harvested more energy to forward the signal. These results verify that the IoT network according to our proposal improve the service for the far user.

The analysis (Ana) OP results (bigger-markers) achieved at D_1 and D_2 in HD-IoT network were obtained from (24) and (40), respectively, and were verified by Monte Carlo simulation (Sim) results (solid-lines) obtained from (23) and (39), where $\varphi = HD$. We also applied min-rate frameworks to investigate OP performances at the devices. The theoretical min-rate OP results (smaller-markers) achieved at devices D_1 and D_2 were obtained from (29) or (30) and (43), respectively. The theoretical min-rate OP performances were verified by min-rate Algorithm 2 results (dashed-lines) at devices D_1 from (27) or (28) and at D_2 from (42), where $\varphi = HD$. The approximate min-rate OP results (crossed-dotted lines) achieved at devices D_1 and D_2 were obtained from (33) or (34) and (45), respectively. We may observe that the approximate min-rate OP results match the theoretical and simulated min-rate OP results perfectly, where SNR $\rho \to \infty$.

In Figure 6a, device D_1 with a fixed PS factor offered better performance with the PS factor from (58), in contrast with device D_2. However, the far device D_2 with PS factor from (58) obtained better performance, as shown in Figure 6b. IoT networks must ensure performance for the entire system (both near and far devices). However, it is trade off. If one device obtains better performance, another device obtains worse performance. The present study's third contribution is therefore in ensuring QoS for both the near and far devices. To prove this aim, we investigated Jain's index fairness in (64) and user throughput fairness in (65), plotted in Figure 9. We may observe that the fairness performance with PS in (58) provided the best performance. An investigation of the results showed that both the near and far devices obtained the same QoS. Finally, we may also conclude that the proposed adaptive PS factor serving the far device is better than the fixed PS factor.

3) OP PERFORMANCE AT THE DEVICES IN THE FD-IoT NETWORK MODEL

In this subsection, we investigate the OP performances at devices D_1 and D_2, where D_1 functions in FD mode to reduce latency at device D_2 as the second aim. As indicated in the PS diagram in Figure 1b, the larger PS factor ε better serves the far device D_2 in HD scenario. However, we adopted an FD relay (Figure 2a) and obtained a resulting PS diagram (Figure 2b). Note that device D_1 in FD scenario was affected by the LI channel as in (5). As a result, the larger PS factor $\varepsilon^{(FD)}$ led to a larger LI. Thus, the SINRs given by (6) and (7), obtained when D_1 decodes data symbols x_2 and x_1, respectively, were less than the SINRs given by (2) and (3) at the same SNR. We therefore adjusted the PS factor $\varepsilon^{(FD)}$ in (59) to reduce diffraction at device D_1 and also to maintain QoS at device D_2. To illustrate, in the HD scenario, we constrained the SINRs $\gamma_{1-x_1}^{(HD)} = \gamma_{2-x_2}^{(HD)}$ given by (57) and exploited the PS allocation $0.5 < \varepsilon^{(HD)} < 1$. If we reuse the PS factor $\varepsilon^{(HD)}$ in the FD scenario, it can lead to an large effect by the LI channel on OP performance at D_1. We therefore propose a PS factor which adopts an FD scenario as given by (59). As a result, we obtain $0.5 < \varepsilon^{(FD)} < \varepsilon^{(HD)} < 1$. Figures 7a and 7b

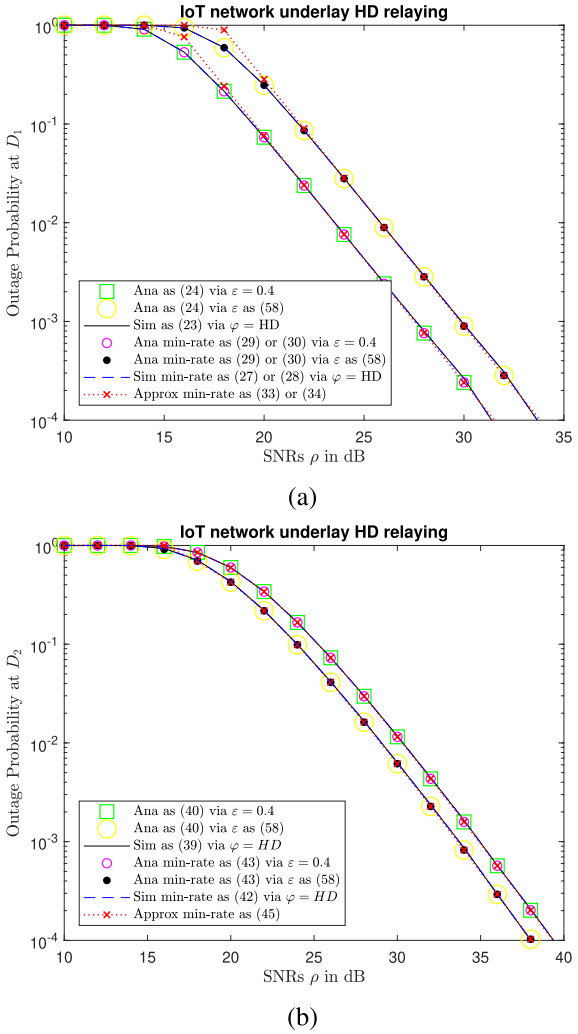

FIGURE 6. OP performance over an HD-IoT network at (a) near device D_1 and (b) far device D_2.

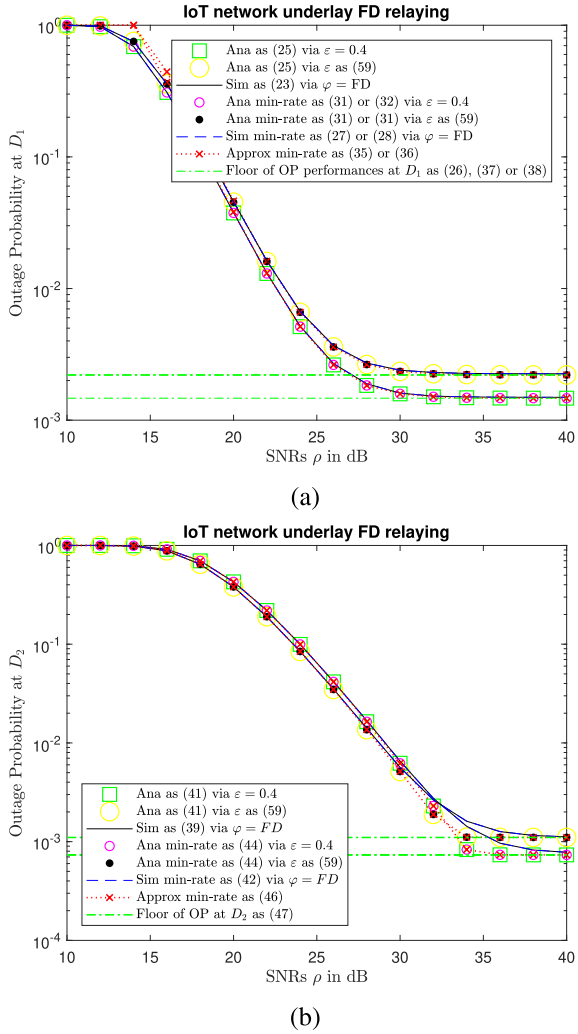

FIGURE 7. OP performance over an FD-IoT network at (a) near device D_1 and (b) far device D_2.

depict OP performance at devices D_1 and D_2, respectively, where D_1 adopted FD mode.

In an HD scenario, the OP performance will tend toward zero when SNR $\rho \to \infty$, as shown in Figure 6. However, Figures 7a and 7b plot the OP performances at the near and far devices for the FD scenario, where the performances did not change at high SNRs. For clarity, we consider equation (5), which is the received signal at device D_1. Device D_1 not only receives a signal from source S but also receives LI. However, LI refers to the EH expression in (56). Therefore, a higher PS factor and higher SNR will lead to higher LI. As a result, OP performance at devices D_1 and D_2 will tend toward their floor OP results (green dashed-dotted lines) when SNR $\rho \to \infty$. We exploited the floor OP at device D_1 as given in (26), (37) or (38) and device D_2 in (47).

For a general perspective, we examined the OP performances given by (62) on the y-axis at left and throughput performances given by (63) on the y-axis at right, where $\varphi = \{HD, FD\}$ (Figure 8). The black-circle markers and dotted-lines plot the best theoretical and simulated OP results of an FD-IoT network model with PS factor $\varepsilon^{(FD)} = 0.5005$ given by (59) at low SNR, i.e., $\rho \leq 30\ dB$. The HD-IoT network model with PS factor $\varepsilon^{\{HD\}}$ given by (58) always attained better OP performance than the same scenario with fixed PS factor $\varepsilon = 04$. These results verify the efficiency of the hypothesized PS factors for the SWIPT models. However, it is very interesting that the OP results of the HD-IoT scenario with PS factor $\varepsilon^{(HD)}$ obtained better OP performances with fixed PS factor $\varepsilon = 0.4$ (left y-axis) yet worse throughput performances (right y-axis) at low SNR, i.e., $\rho \leq 20\ dB$. To illustrate, we may observe that the OP performance at device D_1 in the HD scenario with fixed PS factor $\varepsilon = 0.4$ (Figure 6a) significantly outperformed the OP at device D_2 also in the HD scenario with fixed PS factor $\varepsilon = 0.4$ (Figure 6b). This indicates that the devices in HD scenarios with fixed PS $\varepsilon = 0.4$ were not served with QoS fairness at low SNRs, i.e., from (63), we obtained $T^{(HD,\varepsilon=0.4)} = \left(1 - \mathcal{O}_1^{(HD,\varepsilon=0.4)}\right) R_1 + \left(1 - \mathcal{O}_2^{(HD,\varepsilon=0.4)}\right) R_2 \approx \left(1 - \mathcal{O}_1^{(HD,\varepsilon=0.4)}\right) R_1$ due to

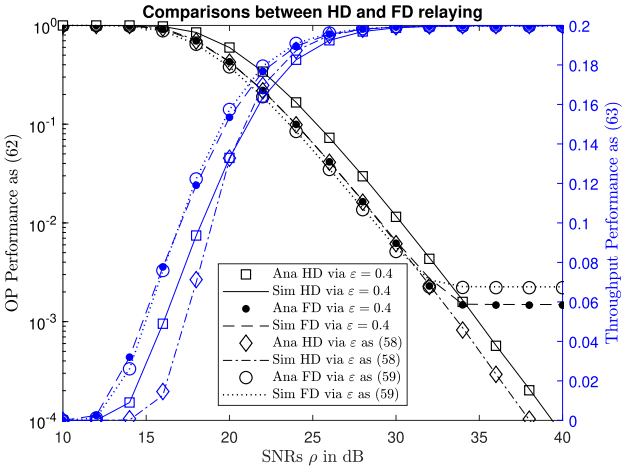

FIGURE 8. The y-axis at left depicts OP performances obtained from (62); the y-axis at right depicts throughput performance obtained from (63), for scenarios $\varphi = \{HD, FD\}$ and PS cases $\varepsilon = \{0.4, (58), (59)\}$.

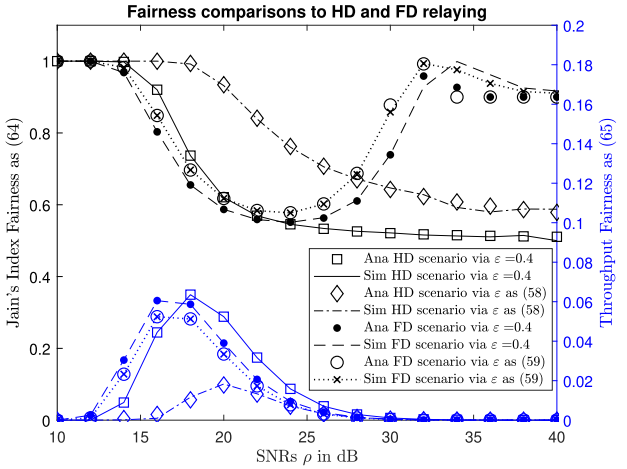

FIGURE 9. QoS fairness of the individual scenarios.

$\mathcal{O}_2^{(HD,\varepsilon=0.4)} \approx 1$ at low SNR, i.e., $\rho \leq 20\ dB$. Although affected by LI, FD scenario with $\varepsilon^{(FD)} = 0.5005$ achieved the best OP performance compared to the individual scenarios with both HD and FD relays using PS factors $\varepsilon = 0.4$ and $\varepsilon^{(HD)} = 0.8389$ at low SNR, e.g. $\rho < 30\ dB$. The throughput performances in individual FD scenarios achieved better throughput performance than HD scenarios in almost SNR periods that achieved their bit-rate thresholds $T^{(\varphi)} = R_1 + R_2 = 0.2\ bps/Hz$.

B. QoS FAIRNESS

The main aim in this study was to guarantee QoS for both the near and far devices. The OP performances of the devices are thus required approximately together. Figure 9 depicts the QoS fairness of devices based on Jain's index fairness given by (64) and throughput fairness obtained from (65), indicated on the black left y-axis and the blue right y-axis, respectively. The results from Jain's index fairness show that the higher results have better fairness OP performance. The Jain's index fairness result with PS factor $\varepsilon^{(HD)}$ is significantly outperformed than the result with fixed PS factor $\varepsilon = 0.4$ in HD scenario. Similarly, the Jain's index fairness result with PS factor $\varepsilon^{(FD)}$ is always better than the result with fixed PS factor $\varepsilon = 0.4$ in FD scenario. Since the results Jain's index fairness show that the higher results have better fairness performance. We can observe that the Jain's index fairness performance obtained in the HD/FD scenarios with a PS factors given by (58) and (59) significantly outperform the same scenarios with fixed PS factor $\varepsilon = 0.4$.

Beside, we plotted the throughput fairness results (blue y-axis at right) as (65) in HD/FD-IoT networks with PS factors $\varepsilon = 0.4$, $\varepsilon^{(HD)}$ and $\varepsilon^{(FD)}$.

To illustrate, we inspected the difference of throughput fairness of the devices by using (65). Extracting the analysis results, we exploited the throughput fairness peaks of the individual scenarios as follows:

$$\max_{\rho=\{10,\ldots,40\}} \left\{\mathcal{T}^{(HD,\varepsilon=0.4)}\right\} = 0.0636\ bps/Hz \text{ for } \rho = 18\ dB,$$

$$\max_{\rho=\{10,\ldots,40\}} \left\{\mathcal{T}^{(HD,\varepsilon=0.8389)}\right\} = 0.0178\ bps/Hz \text{ for } \rho = 20\ dB,$$

$$\max_{\rho=\{10,\ldots,40\}} \left\{\mathcal{T}^{(FD,\varepsilon=0.4)}\right\} = 0.0605\ bps/Hz \text{ for } \rho = 16\ dB,$$

$$\max_{\rho=\{10,\ldots,40\}} \left\{\mathcal{T}^{(FD,\varepsilon=0.5005)}\right\} = 0.0524\ bps/Hz \text{ for } \rho = 16\ dB.$$

These results show that our proposals are suitable for future IoT networks to serve devices with QoS fairness.

C. SECRECY OP PERFORMANCE

In another major part of this study, we assume that the IoT network presented passive eavesdroppers E_1 near device D_1 to eavesdrop D_1 and E_2 near D_2 to eavesdrop D_2. Some major studies related to the PLS issue in wireless communications have been conducted. In [22], [39]–[41], the authors investigated and improved secrecy OP performance using MISO and MIMO in combination with the TAS protocol. In [43], the authors improved the secrecy OP performance by increasing the number of relays or Nakagami-m coefficient. The authors in work [45] examined SIMO secrecy OP performance in combination with SWIPT. However, the work in this study was significantly different to previous studies. Figure 3 shows a model using SISO and a single relay. In our study, however, we focus on PS diagram designs and prove that the PS factors may also improve secrecy OP performance. Figures 10a and 10b plot the secrecy OP performance at devices D_1 and D_2 in individual scenarios. It is interesting that the secrecy OP performances at the devices in an FD-IoT network achieve better performance than in an HD-IoT network. In addition, the secrecy OP at device D_2 with PS factors given by (58) and (59) outperforms itself when the PS factor is set to $\varepsilon = 0.4$. These results prove that the PS factors may combat the eavesdroppers. Note that the simulated secrecy

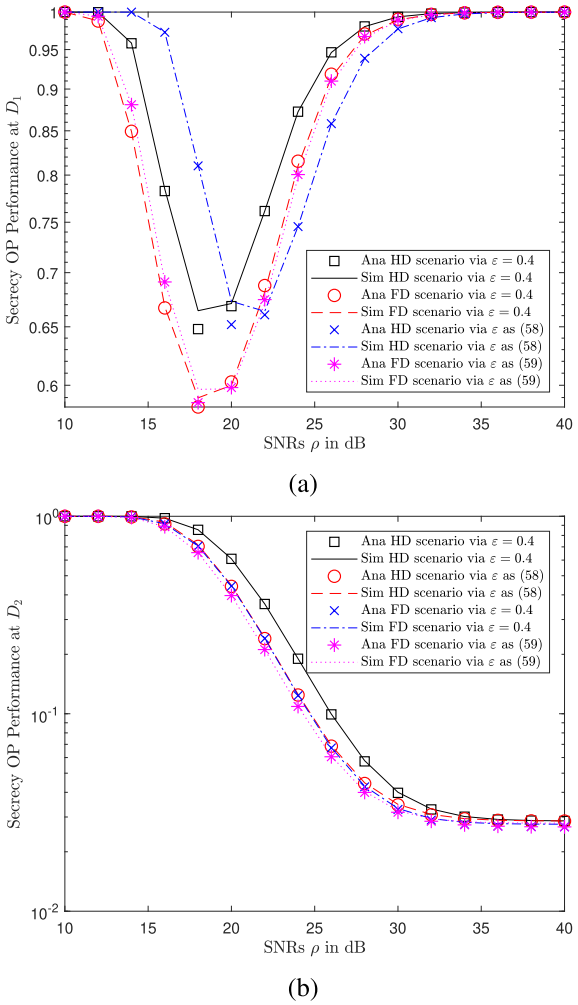

FIGURE 10. Secrecy OP performance at (a) device D_1 with eavesdropper E_1 and (b) device D_2 with only eavesdropper E_2 (without eavesdropper E_1).

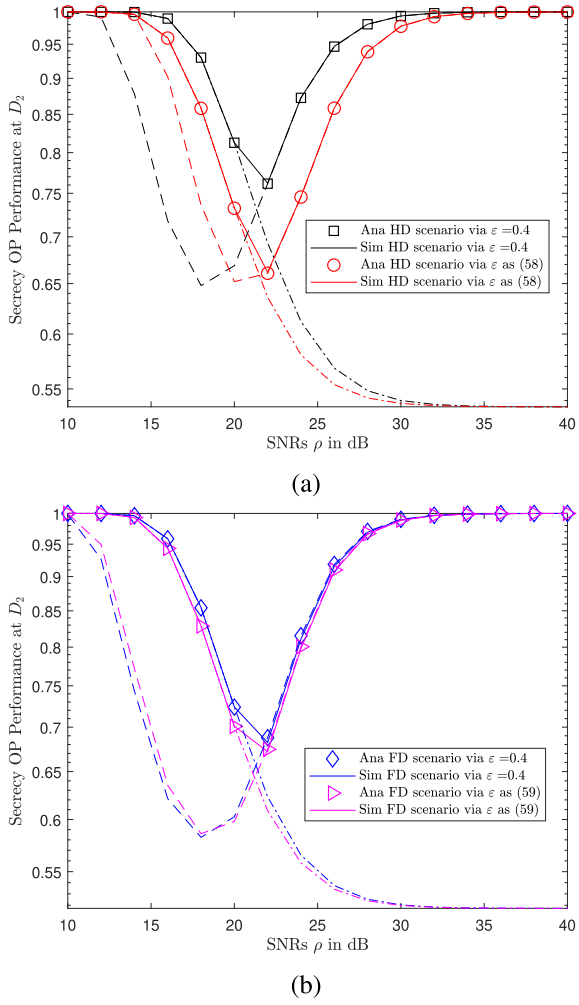

FIGURE 11. Secrecy OP performance at device D_2 with two eavesdroppers in (a) HD-IoT networks and (b) FD-IoT networks.

OP performances at devices D_1 and D_2 obtained by (49) and (53) are used to verify the respective theoretical secrecy OP performances obtained by (50), (51), (54) and (55).

In Figure 7a, it is interesting to observe that the OP performance at device D_1 in an FD-IoT network may be improved by increasing the SNR. However, OP performance at device D_1 in an FD-IoT network is limited by the floor of the OP performance, as given by (26), (37) or (38) due to the effect of LI. Specifically, in a secret FD-IoT network, device D_1 is affected not only by LI but also the eavesdropper E_1. Note that the eavesdropper received the signal as (12) and then SIC as (13) and (14) without the effect of LI. Therefore, the eavesdropper E_1 may successfully decode the messages in a superimposed signal (12) if SNR $\rho \to \infty$. As a result, the secrecy OP performance at device D_1 in an FD-IoT network (Figure 7a) may tend toward one since the secrecy instantaneous bit-rate threshold as given by (16) tends toward zero if SNR $\rho \to \infty$.

Figures plot secrecy OP results at device D_2 in HD-IoT networks (Figure 11a) and FD-IoT networks (Figure 11b). It is different to the secrecy OP results at device D_2 in HD/FD IoT networks without eavesdropper E_1 as shown Figure 10b. Therefore, the results in Figure 10b were only depended to the OP at device D_1. And, the secrecy OP results at device D_2 were not changed at high SNR, i.e., $\rho > 30\ dB$. However, the secrecy OP results shown in Figure 11a and 11b tend to one if SNR $\rho \to \infty$. To illustrate, we investigate the secrecy OP results at device D_1 when device D_1 cannot successfully decode x_2 under impact from eavesdropper E_1 (dashed lines) and secrecy OP results at device D_2 when device D_2 cannot successfully decode x_2 under impact from eavesdropper E_2 (dashed-dotted lines). Finally, we plot the secrecy OP results at device D_2 (solid lines and various markers). It is quite interesting. The secrecy OP results at device D_2 at low SNR, i.e., $\rho < 22\ dB$, refer to the secrecy OP results when secrecy instantaneous bit-rate $R_2^{(\varphi)}$ of device D_2 cannot reach data rate threshold R. However, the secrecy OP results at device D_1 at high SNR, i.e., $\rho > 22\ dB$, refer to the secrecy OP results when secrecy instantaneous bit-rate $R_{1-x_2}^{(\varphi)}$ of device D_1 cannot reach data rate threshold R. It is important to notice that the secrecy OP results in HD/FD IoT networks with PS

factors given by (58) and (59) are better the results in the same individual scenarios with fixed PS factors. It means that the proposed PS diagrams as shown Figures 1b and 2b may combat the eavesdroppers better.

V. CONCLUSION

We hypothesized that the EH in SWIPT can be used to forward signals. We designed an IoT network underlay cooperative NOMA in combination with SWIPT. To reach ultra-low latency, we designed a novel PS diagram. In the results, we obtained novel expressions in accurate and approximate closed-forms. By applying the PS diagrams based on balancing EH and signal processing, the system performance of IoT networks achieved better OP performance, throughput, fairness and secrecy OP. An analysis of the results verified that the PS balanced the model not only in assisting the far device but also guaranteeing the fairness of QoS of the devices in the IoT networks. The analysis results were proved and verified by Monte Carlo simulation results and may be applied to future green and secure IoT networks. In fact, the system performances of the HD/FD IoT networks in this study may be significantly improved by equipping multiple antennae at network nodes or distributing over Nakagami-m fading channels.

APPENDIX A
PROOF OF THEOREM 1

From (23) for $\varphi = HD$, we obtain

$$OP_1^{(HD)} = \underbrace{\Pr\left\{\gamma_{1-x_2}^{(HD)} < \gamma_2^{(HD)}\right\}}_{Q_1} + \underbrace{\Pr\left\{\gamma_{1-x_2}^{(HD)} \geq \gamma_2^{(HD)}, \gamma_{1-x_1}^{(HD)} < \gamma_1^{(HD)}\right\}}_{Q_2}. \quad (66)$$

After some algebraic manipulation, we obtain:

$$Q_1 = \Pr\left\{|h_1|^2 < \frac{\gamma_2^{(HD)}}{\xi^{(HD)}\left(\alpha_2 - \alpha_1\gamma_2^{(HD)}\right)\rho}\right\}. \quad (67)$$

By applying the CDF given by (22), the expression (67) may be obtained:

$$\begin{aligned} Q_1 &= F_{|h_1|^2}(x) \\ &= 1 - \exp\left(-\frac{\gamma_2^{(HD)}}{\xi^{(HD)}\left(\alpha_2 - \alpha_1\gamma_2^{(HD)}\right)\rho\sigma_1}\right). \end{aligned} \quad (68)$$

The expression Q_2 in (66) can be rewritten as follows:

$$Q_2 = \Pr\left\{|h_1|^2 \geq \frac{\gamma_2^{(HD)}}{\xi^{(HD)}\left(\alpha_2 - \gamma_2^{(HD)}\alpha_1\right)\rho}, |h_1|^2 < \frac{\gamma_1^{(HD)}}{\xi^{(HD)}\alpha_1\rho}\right\}. \quad (69)$$

Similarly, we may obtain Q_2 in closed-form by applying the CDF given (21) as follows:

$$\begin{aligned} Q_2 &= \int_{\frac{\gamma_2^{(HD)}}{\xi^{(HD)}\left(\alpha_2-\gamma_2^{(HD)}\alpha_1\right)\rho}}^{\frac{\gamma_1^{(HD)}}{\xi^{(HD)}\alpha_1\rho}} \frac{1}{\sigma_1}\exp\left(-\frac{y}{\sigma_1}\right)dy \\ &= \exp\left(-\frac{\gamma_2^{(HD)}}{\xi^{(HD)}\left(\alpha_2 - \gamma_2^{(HD)}\alpha_1\right)\rho\sigma_1}\right) \\ &\quad - \exp\left(-\frac{\gamma_1^{(HD)}}{\xi^{(HD)}\alpha_1\rho\sigma_1}\right), \end{aligned} \quad (70)$$

where $\alpha_2 - \gamma_2^{(HD)}\alpha_1 > \alpha_1$.

By substituting (68) and (70) into (66), we obtain the OP at the near device D_1 in HD scenario in closed-form, as shown in (24).

In the FD-IoT model, the near device D_1 works in FD relaying mode. The near device D_1 has to decode messages x_2 and x_1 according to (6) and (7), respectively, under the impact of the LI channel. From (23) for $\varphi = FD$, the OP at the near device D_1 in the FD-IoT model is expressed as follows:

$$OP_1^{(FD)} = \underbrace{\Pr\left\{\gamma_{1-x_2}^{(FD)} < \gamma_2^{(FD)}\right\}}_{Q_3} + \underbrace{\Pr\left\{\gamma_{1-x_2}^{(FD)} \geq \gamma_2^{(FD)}, \gamma_{1-x_1}^{(FD)} < \gamma_1^{(FD)}\right\}}_{Q_4}. \quad (71)$$

Let $\sigma_{LI} = E\left\{|h_{LI}|^2\right\} = \varpi E\left\{|h_1|^2\right\}$. After some algebraic manipulation, we obtain:

$$Q_3 = 1 - \Pr\left\{\begin{array}{l} |h_1|^2 \geq \frac{\gamma_2^{(FD)}\left(\eta^2|h_{LI}|^2\varepsilon^{(FD)}\rho+1\right)}{\xi^{(FD)}\rho\left(\alpha_2-\alpha_1\gamma_2^{(FD)}\right)}, \\ |h_{LI}|^2 \geq 0 \end{array}\right\}. \quad (72)$$

By applying the PDF as given by (21), we obtain

$$\begin{aligned} Q_3 &= 1 - \int_0^{\infty}\int_{\frac{\gamma_2^{(FD)}\left(\eta^2 y\varepsilon^{(FD)}\rho+1\right)}{\xi^{(FD)}\left(\alpha_2-\alpha_1\gamma_2^{(FD)}\right)\rho}}^{\infty} \frac{1}{\varpi\sigma_1^2} \\ &\quad \times \exp\left(-\frac{x}{\sigma_1} - \frac{y}{\varpi\sigma_1}\right)dxdy \\ &= 1 - \exp\left(-\frac{\gamma_2^{(FD)}}{\xi^{(FD)}\left(\alpha_2 - \alpha_1\gamma_2^{(FD)}\right)\rho\sigma_1}\right) \\ &\quad \times \frac{\xi^{(FD)}\left(\alpha_2 - \alpha_1\gamma_2^{(FD)}\right)}{\xi^{(FD)}\left(\alpha_2 - \alpha_1\gamma_2^{(FD)}\right) + \eta^2\varpi\varepsilon^{(FD)}\gamma_2^{(FD)}}, \end{aligned} \quad (73)$$

where $R_2 < \frac{1}{2}\log_2\left(\frac{\alpha_2-\alpha_1}{\alpha_1}+1\right)$.

The expression Q_4 in (71) is obtained by

$$Q_4 = \Pr\left\{|h_1|^2 \geq \frac{\gamma_2^{(FD)}\left(\eta^2|h_{LI}|^2\varepsilon^{(FD)}\rho+1\right)}{\xi^{(FD)}\left(\alpha_2-\alpha_1\gamma_2^{(FD)}\right)\rho}, |h_1|^2 < \frac{\gamma_1^{(FD)}\left(\eta^2|h_{LI}|^2\varepsilon^{(FD)}\rho+1\right)}{\xi^{(FD)}\alpha_1\rho}, |h_{LI}|^2 \geq 0\right\}. \quad (74)$$

Similarly, the expression Q_6 in (67) can be obtained in closed-form as follows:

$$\begin{aligned} &Q_4 \\ &= \int_0^{\infty} \int_{\frac{\gamma_2^{(FD)}\left(\eta^2 y\varepsilon^{(FD)}\rho+1\right)}{\xi^{(FD)}\left(\alpha_2-\alpha_1\gamma_2^{(FD)}\right)\rho}}^{\frac{\gamma_1^{(FD)}\left(\eta^2 y\varepsilon^{(FD)}\rho+1\right)}{\xi^{(FD)}\alpha_1\rho}} \frac{1}{\sigma_1\sigma_{LI}}\exp\left(-\frac{x}{\sigma_1}-\frac{y}{\sigma_{LI}}\right)dxdy \\ &= \xi^{(FD)}\left(\exp\left(-\frac{\gamma_2^{(FD)}}{\xi^{(FD)}\left(\alpha_2-\alpha_1\gamma_2^{(FD)}\right)\rho\sigma_1}\right)\right. \\ &\quad\times\frac{\alpha_2-\alpha_1\gamma_2^{(FD)}}{\xi^{(FD)}\left(\alpha_2-\alpha_1\gamma_2^{(FD)}\right)+\gamma_2^{(FD)}\eta^2\varepsilon^{(FD)}\varpi} \\ &\quad\left.-\exp\left(-\frac{\gamma_1^{(FD)}}{\xi^{(FD)}\alpha_1\rho\sigma_1}\right)\frac{\alpha_1}{\xi^{(FD)}\alpha_1+\gamma_1^{(FD)}\eta^2\varepsilon^{(FD)}\varpi}\right), \end{aligned} \quad (75)$$

where $R_2 < \log_2\left(\frac{\alpha_2-\alpha_1}{\alpha_1}+1\right)$.

By substituting (73) and (75) into (71), we obtain the OP at the near device D_1 in the FD-IoT model in closed form given by (25).

APPENDIX B
PROOF OF LEMMA 1

From (27) and (28), we obtain min-rate OP at device D_1 in the HD scenario as follows:

$$\begin{aligned} &MOP_1^{(HD)} \\ &= 1-\min\left\{\Pr\left\{|h_1|^2 \geq \frac{\gamma_2^{(HD)}}{\xi^{(HD)}\left(\alpha_2-\alpha_1\gamma_2^{(HD)}\right)\rho}\right\}, \right. \\ &\quad\left.\Pr\left\{|h_1|^2 \geq \frac{\gamma_1^{(HD)}}{\xi^{(HD)}\alpha_1\rho}\right\}\right\} \\ &= 1-\Pr\left\{|h_1|^2 \geq \frac{\max\left\{\frac{\gamma_2^{(HD)}}{\alpha_2-\alpha_1\gamma_2^{(HD)}}, \frac{\gamma_1^{(HD)}}{\alpha_1}\right\}}{\xi^{(HD)}\rho}\right\} \\ &= 1-f_{|h_1|^2}(x) \\ &= 1-\exp\left(-\frac{\max\left\{\frac{\gamma_2^{(HD)}}{\alpha_2-\alpha_1\gamma_2^{(HD)}}, \frac{\gamma_1^{(HD)}}{\alpha_1}\right\}}{\xi^{(HD)}\rho\sigma_1}\right) \\ &= 1-\exp\left(-\frac{\gamma^{(HD)}}{\xi^{(HD)}\rho\sigma_1\min\left\{\frac{\alpha_2-\alpha_1\gamma^{(HD)}}{\alpha_1}\right\}}\right). \end{aligned} \quad (76)(77)$$

such that $R_1 \neq R_2$ in (76) and $R_1 = R_2 = R$ in (77).

Similarly, from (27) and (28), where $\varphi = FD$, we may obtain the min-rate OP at device D_1 in FD scenario as follows:

$$\begin{aligned} &MOP_1^{(FD)} \\ &= 1-\min\left\{\Pr\left\{|h_1|^2 \geq \frac{\gamma_1^{(FD)}\left(\eta^2|h_{LI}|^2\varepsilon^{(FD)}\rho+1\right)}{\xi^{(FD)}\alpha_1\rho}, \right.\right. \\ &\quad\left.|h_{LI}|^2 \geq 0\right\}, \\ &\quad\Pr\left\{|h_1|^2 \geq \frac{\gamma_2^{(FD)}\left(\eta^2|h_{LI}|^2\varepsilon^{(FD)}\rho+1\right)}{\xi^{(FD)}\left(\alpha_2-\alpha_1\gamma_2^{(FD)}\right)\rho}, \right. \\ &\quad\left.\left.|h_{LI}|^2 \geq 0\right\}\right\}. \end{aligned} \quad (78)$$

We obtain

$$\begin{aligned} &MOP_1^{(FD)} \\ &= 1-\int_0^{\infty}\int_{\frac{\eta^2 y\varepsilon^{(FD)}\rho+1}{\xi^{(FD)}\rho}\max\left\{\frac{\gamma_2^{(FD)}}{\alpha_2-\alpha_1\gamma_2^{(FD)}}, \frac{\gamma_1^{(FD)}}{\alpha_1}\right\}}^{\infty} \frac{1}{\varpi\sigma_1^2} \\ &\quad\times\exp\left(-\frac{x}{\sigma_1}-\frac{y}{\varpi\sigma_1}\right)dxdy \\ &= 1-\exp\left(-\frac{\max\left\{\frac{\gamma_2^{(FD)}}{\alpha_2-\alpha_1\gamma_2^{(FD)}}, \frac{\gamma_1^{(FD)}}{\alpha_1}\right\}}{\xi^{(FD)}\rho\sigma_1}\right) \\ &\quad\times\frac{\xi^{(FD)}}{\xi^{(FD)}+\eta^2\varpi\varepsilon^{(FD)}\max\left\{\frac{\gamma_2^{(FD)}}{\alpha_2-\alpha_1\gamma_2^{(FD)}}, \frac{\gamma_1^{(FD)}}{\alpha_1}\right\}} \\ &= 1-\exp\left(-\frac{\gamma^{(FD)}}{\xi^{(FD)}\rho\sigma_1\min\left\{\frac{\alpha_2-\alpha_1\gamma^{(HD)}}{\alpha_1}\right\}}\right) \\ &\quad\times\frac{\xi^{(FD)}\min\left\{\alpha_2-\alpha_1\gamma^{(FD)}, \alpha_1\right\}}{\xi^{(FD)}\min\left\{\alpha_2-\alpha_1\gamma^{(FD)}, \alpha_1\right\}+\eta^2\varpi\varepsilon^{(FD)}\gamma^{(FD)}}, \end{aligned} \quad (79)(80)$$

such that $R_1 \neq R_2$ in (79) and $R_1 = R_2 = R$ in (80).

APPENDIX C
PROOF OF THEOREM 2

From (39) for $\varpi = HD$, we obtain the OP at the far device D_2 in the HD-IoT model as follows:

$$OP_2^{(HD)} = \underbrace{\Pr\left\{\gamma_{1-x_2}^{(HD)} < \gamma_2^{(HD)}\right\}}_{Q_1} + \underbrace{\Pr\left\{\gamma_{1-x_2}^{(HD)} \geq \gamma_2^{(HD)}, \gamma_{2-x_2}^{(HD)} < \gamma_2^{(HD)}\right\}}_{Q_5}. \quad (81)$$

However, it is important to note that the expression Q_5 has two randomly independent variables. By applying the PDF given by (21), we obtain

$$\begin{aligned} Q_5^{(HD)} &= 1 - \Pr\left\{ |h_1|^2 \geq \frac{\gamma_2^{(HD)}}{\xi^{(HD)}\left(\alpha_2 - \alpha_1\gamma_2^{(HD)}\right)\rho}, \right. \\ &\quad \left. |h_1|^2 < \frac{\gamma_2^{(HD)}}{\eta^2|h_2|^2\varepsilon^{(HD)}\rho}, |h_2|^2 > 0 \right\} \\ &= \int_0^{\infty} \int_{\frac{\gamma_2^{(HD)}}{\xi^{(HD)}\left(\alpha_2-\alpha_1\gamma_2^{(HD)}\right)\rho}}^{\frac{\gamma_2^{(HD)}}{\eta^2 y\varepsilon^{(HD)}\rho}} \frac{1}{\sigma_1\sigma_2}\exp\left(-\frac{x}{\sigma_1} - \frac{y}{\sigma_2}\right)dxdy \\ &= \exp\left(-\frac{\gamma_2^{(HD)}}{\xi^{(HD)}\left(\alpha_2 - \alpha_1\gamma_2^{(HD)}\right)\rho\sigma_1}\right) \\ &\quad - \frac{2B_1\left\{2\Big/\sqrt{\frac{\eta^2\varepsilon^{(HD)}\rho\sigma_1\sigma_2}{\gamma_2^{(HD)}}}\right\}}{\sqrt{\frac{\eta^2\varepsilon^{(HD)}\rho\sigma_1\sigma_2}{\gamma_2^{(HD)}}}}. \end{aligned} \tag{82}$$

By substituting (68) and (82) into (81), we obtain the OP at the far device D_2 in the HD-IoT model in closed form given by (40).

However, the OP at the far device D_2 in the FD-IoT model can be rewritten as follows:

$$\begin{aligned} OP_2^{(FD)} &= \underbrace{\Pr\left\{\gamma_{1-x_2}^{(FD)} < \gamma_2^{(FD)}\right\}}_{Q_4} \\ &\quad + \underbrace{\Pr\left\{\gamma_{1-x_2}^{(FD)} \geq \gamma_2^{(FD)}, \gamma_{2-x_2}^{(FD)} < \gamma_2^{(FD)}\right\}}_{Q_6}, \end{aligned} \tag{83}$$

where the expressions Q_4 is given by (75). And, $Q_7^{(FD)}$ is similarly obtained as follows:

$$\begin{aligned} Q_6 &= \Pr\left\{ |h_1|^2 \geq \frac{\gamma_2^{(FD)}\left(\eta^2|h_{LI}|^2\varepsilon^{(FD)}\rho + 1\right)}{\xi^{(FD)}\left(\alpha_2 - \alpha_1\gamma_2^{(FD)}\right)\rho}, \right. \\ &\quad \left. |h_1|^2 < \frac{\gamma_2^{(FD)}}{\eta^2|h_2|^2\varepsilon^{(FD)}\rho}, |h_{LI}|^2 \geq 0, |h_2|^2 > 0 \right\} \\ &= \left[\int_0^{\infty}\int_0^{\infty} \int_{\frac{\gamma_2^{(FD)}\left(\eta^2 z\varepsilon^{(FD)}\rho+1\right)}{\xi^{(FD)}\left(\alpha_2-\alpha_1\gamma_2^{(FD)}\right)\rho}}^{\frac{\gamma_2^{(FD)}}{\eta^2 y\varepsilon^{(FD)}\rho}} \frac{1}{\sigma_1\sigma_2\sigma_{LI}} \right. \\ &\quad \left. \times \exp\left(-\frac{x}{\sigma_1} - \frac{y}{\sigma_2} - \frac{z}{\sigma_{LI}}\right)dxdydz \right]^+ \\ &= \left[\exp\left(-\frac{\gamma_2^{(FD)}}{\xi^{(FD)}\left(\alpha_2 - \alpha_1\gamma_2^{(FD)}\right)\rho\sigma_1}\right) \right. \\ &\quad \left. \times \frac{\xi^{(FD)}\left(\alpha_2 - \alpha_1\gamma_2^{(FD)}\right)\sigma_1}{\xi^{(FD)}\left(\alpha_2 - \alpha_1\gamma_2^{(FD)}\right)\rho\sigma_1 + \gamma_2^{(FD)}\eta^2\varepsilon^{(FD)}\sigma_{LI}} \right. \\ &\quad \left. - \frac{2B_1\left\{2\Big/\sqrt{\frac{\eta^2\varepsilon^{(FD)}\rho\sigma_1\sigma_2}{\gamma_2^{(FD)}}}\right\}}{\sqrt{\frac{\eta^2\varepsilon^{(FD)}\rho\sigma_1\sigma_2}{\gamma_2^{(FD)}}}} \right]^+. \end{aligned} \tag{84}$$

By substituting (75) and (84) into (83), we obtain the OP at the far device D_2 in FD-IoT model in closed form as given by (41).

APPENDIX D
PROOF OF THEOREM 3

The secrecy OP performance at device D_1 is given by (48) and (49), where $\varphi = HD$.

From Q_3 and Q_1 in (73) and (68), we obtain the CDF of devices D_1 and eavesdropper E_1 when they decode the data symbolsx_1 and x_2, respectively, as follows:

$$F_{\gamma_{d-x_1}^{(HD)}}(x) = 1 - \exp\left(-\frac{x}{\xi^{(HD)}\alpha_1\rho\sigma_d}\right), \tag{85}$$

and

$$\begin{aligned} &F_{\gamma_{d-x_2}^{(HD)}}(x) \\ &= \begin{cases} 1 - \exp\left(-\dfrac{x}{\xi^{(HD)}\left(\alpha_2 - \alpha_1 x\right)\rho\sigma_d}\right), & x < \dfrac{\alpha_2}{\alpha_1}, \\ 1, & x \geq \dfrac{\alpha_2}{\alpha_1}, \end{cases} \end{aligned} \tag{86}$$

where $d = \{1, 3\}$.

We obtain the PDF of devices D_1 and eavesdropper E_1 when they decode the x_2 and x_1 data symbols, respectively, as follows:

$$f_{\gamma_{d-x_1}^{(HD)}}(x) = \frac{\exp\left(-\frac{x}{\xi^{(HD)}\alpha_1\rho\sigma_d}\right)}{\xi^{(HD)}\alpha_1\rho\sigma_d}, \tag{87}$$

and

$$\begin{aligned} &f_{\gamma_{d-x_2}^{(HD)}}(x) \\ &= \begin{cases} \dfrac{\alpha_2\exp\left(-\frac{x}{\xi^{(HD)}(\alpha_2-\alpha_1 x)\rho\sigma_d}\right)}{\xi^{(HD)}(\alpha_2 - \alpha_1 x)^2\rho\sigma_d}, & x < \dfrac{\alpha_2}{\alpha_1} \\ 0, & x \geq \dfrac{\alpha_2}{\alpha_1}, \end{cases} \end{aligned} \tag{88}$$

Let $Q_7 = \Pr\left\{\left[R_{1-x_1}^{(HD)} - R_{3-x_1}^{(HD)}\right]^+ \geq R_1\right\}$. From [40, Eq. (9)], the expression Q_7 can be obtained as follows:

$$Q_7 = 1 - \int_0^{\infty} F_{\gamma_{1-x_1}^{(HD)}}\left(\tilde{\gamma}_1^{(HD)}y + \gamma_1^{(HD)}\right) f_{\gamma_{3-x_1}^{(HD)}}(y)\,dy. \tag{89}$$

By substituting (85) and (87) into (89), we obtain

$$Q_7 = \frac{\sigma_1}{\sigma_1 + \tilde{\gamma}_1^{(HD)}\sigma_3}\exp\left(-\frac{\gamma_1^{(HD)}}{\xi^{(HD)}\alpha_1\rho\sigma_1}\right). \tag{90}$$

Let $Q_8 = \Pr\left\{\left[R_{1-x_2}^{(HD)} - R_{3-x_2}^{(HD)}\right]^+ \geq R_2\right\}$.

We then obtain

$$Q_8 = 1 - \int_0^{\psi} F_{\gamma_{1-x_2}^{(HD)}}\left(\tilde{\gamma}_2^{(HD)} y + \gamma_2^{(HD)}\right) f_{\gamma_{3-x_2}^{(HD)}}(y)\, dy + \int_{\psi}^{\alpha_2/\alpha_1} f_{\gamma_{3-x_2}^{(HD)}}(y)\, dy$$
$$= \frac{\alpha_2 \psi \pi}{2K\xi^{(HD)}\rho\sigma_3} \sum_{k=1}^{K} \left(\frac{\sqrt{1-(2\Omega-1)^2}}{(\alpha_2 - \alpha_1\psi\Omega)^2} \times \exp\left(-\frac{\psi\Omega}{\xi^{(HD)}(\alpha_2 - \alpha_1\psi\Omega)\rho\sigma_3}\right) \times \exp\left(-\frac{\tilde{\gamma}_2^{(HD)}\psi\Omega - 1}{\xi^{(HD)}\left(\alpha_2 - \alpha_1\left(\tilde{\gamma}_2^{(HD)}\Omega - 1\right)\right)\rho\sigma_1}\right)\right). \quad (91)$$

By substituting (89) and (91) into (49), we obtain secrecy OP at device D_1 in closed-form as shown (50).

In FD-IoT network model as shown Figure 2a, the secrecy OP performance at device D_1 is given by (48), where $\varphi = FD$.

Let $Q_9 = \Pr\left\{\left[R_{1-x_1}^{(FD)} - R_{3-x_1}^{(FD)}\right]^+ \geq R_1\right\}$.

We then obtain

$$Q_9 = 1 - \int_0^{\infty} F_{\gamma_{1-x_1}^{(FD)}}\left(\tilde{\gamma}_1^{(FD)} y + \gamma_1^{(FD)}\right) f_{\gamma_{3-x_1}^{(FD)}}(y)\, dy$$
$$= -\frac{1}{\eta^2\varepsilon^{(FD)}\varpi\rho\tilde{\gamma}_1^{(FD)}\sigma_3} \exp\left(-\frac{\gamma_1^{(FD)}}{\xi^{(FD)}\alpha_1\rho\sigma_1}\right) \times \left(\exp\left(-\frac{\left(\xi^{(FD)}\alpha_1 + \eta^2\varepsilon^{(FD)}\varpi\gamma_1^{(FD)}\right)\chi}{\xi^{(FD)}\alpha_1\eta^2\varepsilon^{(FD)}\varpi\gamma_1^{(FD)}\rho\sigma_1\sigma_3}\right) \times \left(\lim_{\Gamma\to\infty}\left(\sum_{\gamma=1}^{\Gamma}\frac{1}{\gamma} - \ln\Gamma\right) + \ln\frac{\chi}{\xi^{(FD)}\alpha_1\rho\sigma_1\sigma_3} - \ln\frac{\eta^2\varepsilon^{(FD)}\varpi\tilde{\gamma}_1^{(FD)}}{\xi^{(FD)}\alpha_1 + \eta^2\varepsilon^{(FD)}\varpi\gamma_1^{(FD)}}\right) - U\left\{1; 1; \frac{\left(\xi^{(FD)}\alpha_1 + \eta^2\varepsilon^{(FD)}\varpi\gamma_1^{(FD)}\right)\chi}{\xi^{(FD)}\alpha_1\eta^2\varepsilon^{(FD)}\varpi\gamma_1^{(FD)}\rho\sigma_1\sigma_3}\right\}\right), \quad (92)$$

where $U\{.;.;.\}$ is Kummer's confluent hypergeometric function and $F_{\gamma_{1-x_1}^{(FD)}}(x)$ is given as follows:

$$F_{\gamma_{1-x_1}^{(FD)}}(x) = 1 - \frac{\xi^{(FD)}\alpha_1}{\xi^{(FD)}\alpha_1 + \eta^2\varepsilon^{(FD)}\varpi x} \times \exp\left(-\frac{x}{\xi^{(FD)}\alpha_1\rho\sigma_1}\right). \quad (93)$$

And, let $Q_{10} = \Pr\left\{\left[R_{1-x_2}^{(FD)} - R_{3-x_2}^{(FD)}\right]^+ \geq R_2\right\}$.

We then obtain

$$Q_{10} = 1 - \int_0^{\delta} F_{\gamma_{1-x_2}^{(FD)}}\left(\tilde{\gamma}_2^{(FD)} y + \gamma_2^{(FD)}\right) f_{\gamma_{3-x_2}^{(FD)}}(y)\, dy + \int_{\delta}^{\alpha_2/\alpha_1} f_{\gamma_{3-x_2}^{(FD)}}(y)\, dy$$
$$= \frac{\alpha_2\delta\pi}{2K\xi^{(FD)}\rho\sigma_3 + \eta^2\varepsilon^{(FD)}\varpi\tilde{\gamma}_2^{(FD)}} \times \sum_{k=1}^{K}\left(\frac{\sqrt{1-(2\Omega-1)^2}}{(\alpha_2 - \alpha_1\delta\Omega)^2 + \eta^2\varepsilon^{(FD)}\varpi\tilde{\gamma}_2^{(FD)}} \times \exp\left(-\frac{\delta\Omega}{(1-\varepsilon)(\alpha_2 - \alpha_1\delta\Omega)\rho\sigma_3}\right) \times \exp\left(-\frac{\tilde{\gamma}_2^{(FD)}\delta\Omega - 1}{\xi^{(FD)}\left(\alpha_2 - \alpha_1\left(\tilde{\gamma}_2^{(FD)}\Omega - 1\right)\right)\rho\sigma_3}\right)\right), \quad (94)$$

where $\delta = \frac{1}{\tilde{\gamma}_2^{(FD)}(\alpha_1 + \eta^2\varepsilon^{(FD)}\varpi)} - 1 < \frac{\alpha_2}{\alpha_1}$ and $F_{\gamma_{1-x_2}^{(FD)}}(x)$ is given as follows.

$$F_{\gamma_{1-x_2}^{(FD)}}(x) = 1 - \frac{\xi^{(FD)}(\alpha_2 - \alpha_1 x)}{\xi^{(FD)}(\alpha_2 - \alpha_1 x) + \eta^2\xi^{(FD)}\varpi x} \times \exp\left(-\frac{x}{\xi^{(FD)}(\alpha_2 - \alpha_1 x)\rho\sigma_1}\right). \quad (95)$$

By substituting (92) and (94) into (49), we obtain the secrecy OP at device D_1 in FD scenario in closed-form as shown (51).

APPENDIX E
PROOF OF THEOREM 4

From (53), let $Q_{11}{}^{(\varphi)} = \Pr\left\{\left[R_{2-x_2}^{(\varphi)} - R_{4-x_2}^{(\varphi)}\right]^+ < R_2\right\}$.

After some algebraic, we then obtain

$$Q_{11}^{(\varphi)} = 1 - \Pr\left\{|h_2|^2 \geq \frac{\gamma_2^{(\varphi)} + \left(\gamma_2^{(\varphi)} + 1\right)\eta^2\varepsilon^{(\varphi)}\rho|h_1|^2|h_4|^2}{\eta^2\varepsilon^{(\varphi)}\rho|h_1|^2}, |h_4|^2 \geq 0, |h_1|^2 \geq 0\right\}$$
$$= 1 - \int_0^{\infty}\int_0^{\infty}\int_{\frac{\gamma_2^{(\varphi)} + \left(\gamma_2^{(\varphi)}+1\right)\eta^2\varepsilon^{(\varphi)}\rho zy}{\eta^2\varepsilon^{(\varphi)}\rho z}}^{\infty} \frac{1}{\sigma_1\sigma_2\sigma_4} \times \exp\left(-\frac{x}{\sigma_2} - \frac{y}{\sigma_4} - \frac{z}{\sigma_1}\right) dxdydz$$
$$= 1 - \frac{2\sigma_2 B_1\left(2\Big/\sqrt{\frac{\eta^2\varepsilon^{(\varphi)}\rho\prod_i\sigma_i}{\gamma_2^{(\varphi)}}}\right)}{\sqrt{\frac{\eta^2\varepsilon^{(\varphi)}\rho\prod_i\sigma_i}{\gamma_2^{(\varphi)}}}\left(\sigma_2 + \sigma_4 + \gamma_2^{(\varphi)}\sigma_4\right)}. \quad (96)$$

By substituting (68) and (96) into (53), we obtain secrecy OP at device D_2 in HD scenario as shown (54). And, by substituting (73) and (96) into (53), we obtain secrecy OP at device D_2 in FD scenario without eavesdropper E_1 as shown (55).

REFERENCES

[1] P. Fazio, F. De Rango, and M. Tropea, "Prediction and QoS enhancement in new generation cellular networks with mobile hosts: A survey on different protocols and conventional/unconventional approaches," *IEEE Commun. Surveys Tuts.*, vol. 19, no. 3, pp. 1822–1841, 3rd Quart., 2017.

[2] P. Fazio, F. De Rango, C. Sottile, and C. Calafate, "A new channel assignment scheme for interference-aware routing in vehicular networks," in *Proc. IEEE 73rd Veh. Technol. Conf. (VTC Spring)*, May 2011, pp. 1–5.

[3] S. Zhang, Q. Wu, S. Xu, and G. Y. Li, "Fundamental green tradeoffs: Progresses, challenges, and impacts on 5G networks," *IEEE Commun. Surveys Tuts.*, vol. 19, no. 1, pp. 33–56, Jan./Mar. 2017.

[4] C. Zhu, V. C. M. Leung, L. Shu, and E. C.-H. Ngai, "Green Internet of Things for smart world," *IEEE Access*, vol. 3, pp. 2151–2162, Nov. 2015.

[5] Z. Chu, F. Zhou, Z. Zhu, R. Q. Hu, and P. Xiao, "Wireless powered sensor networks for Internet of Things: Maximum throughput and optimal power allocation," *IEEE Internet Things J.*, vol. 5, no. 1, pp. 310–321, Feb. 2018.

[6] Y. Saito, Y. Kishiyama, A. Benjebbour, T. Nakamura, A. Li, and K. Higuchi, "Non-orthogonal multiple access (NOMA) for cellular future radio access," in *Proc. IEEE 77th Veh. Technol. Conf. (VTC Spring)*, Jun. 2013, pp. 1–5.

[7] Q. C. Li, H. Niu, A. T. Papathanassiou, and G. Wu, "5G network capacity: Key elements and technologies," *IEEE Veh. Technol. Mag.*, vol. 9, no. 1, pp. 71–78, Mar. 2014.

[8] S. M. R. Islam, N. Avazov, O. A. Dobre, and K.-S. Kwak, "Power-domain non-orthogonal multiple access (NOMA) in 5G systems: Potentials and challenges," *IEEE Commun. Surveys Tuts.*, vol. 19, no. 2, pp. 721–742, 2nd Quart., 2017.

[9] Z. Ding, Z. Yang, P. Fan, and H. V. Poor, "On the performance of non-orthogonal multiple access in 5G systems with randomly deployed users," *IEEE Signal Process. Lett.*, vol. 21, no. 12, pp. 1501–1505, Dec. 2014.

[10] T.-N. Tran and M. Voznak, "Multi-points cooperative relay in NOMA system with N-1 DF relaying nodes in HD/FD mode for N user equipments with energy harvesting," *Electronics*, vol. 8, no. 2, p. 167, Feb. 2019.

[11] S. Timotheou and I. Krikidis, "Fairness for non-orthogonal multiple access in 5G systems," *IEEE Signal Process. Lett.*, vol. 22, no. 10, pp. 1647–1651, Oct. 2015.

[12] Z. Wei, J. Yuan, D. W. K. Ng, M. Elkashlan, and Z. Ding, "A survey of downlink non-orthogonal multiple access for 5G wireless communication networks," *ZTE Commun.*, vol. 14, no. 4, pp. 17–23, 2016.

[13] L. Dai, B. Wang, Z. Ding, Z. Wang, S. Chen, and L. Hanzo, "A survey of non-orthogonal multiple access for 5G," *IEEE Commun. Surveys Tuts.*, vol. 20, no. 3, pp. 2294–2323, 3rd Quart., 2018.

[14] L. Pei, Z. Yang, C. Pan, W. Huang, M. Chen, M. Elkashlan, and A. Nallanathan, "Energy-efficient D2D communications underlaying NOMA-based networks with energy harvesting," *IEEE Commun. Lett.*, vol. 22, no. 5, pp. 914–917, May 2018.

[15] F. Fang, H. Zhang, J. Cheng, and V. C. M. Leung, "Energy-efficient resource allocation for downlink non-orthogonal multiple access network," *IEEE Trans. Commun.*, vol. 64, no. 9, pp. 3722–3732, Sep. 2016.

[16] T.-N. Tran and M. Voznak, "On secure system performance over SISO, MISO and MIMO-NOMA wireless networks equipped a multiple antenna based on TAS protocol," *EURASIP J. Wireless Commun. Netw.*, vol. 2020, no. 1, pp. 1–22, Dec. 2020.

[17] J.-B. Kim and I.-H. Lee, "Capacity analysis of cooperative relaying systems using non-orthogonal multiple access," *IEEE Commun. Lett.*, vol. 19, no. 11, pp. 1949–1952, Nov. 2015.

[18] V. Sreng, H. Yanikomeroglu, and D. D. Falconer, "Relayer selection strategies in cellular networks with peer-to-peer relaying," in *Proc. IEEE 58th Veh. Technol. Conf. (VTC-Fall)*, Oct. 2003, pp. 1949–1953.

[19] Y. Jing and H. Jafarkhani, "Single and multiple relay selection schemes and their achievable diversity orders," *IEEE Trans. Wireless Commun.*, vol. 8, no. 3, pp. 1414–1423, Mar. 2009.

[20] S. Lee, D. B. da Costa, Q.-T. Vien, T. Q. Duong, and R. T. de Sousa, "Non-orthogonal multiple access schemes with partial relay selection," *IET Commun.*, vol. 11, no. 6, pp. 846–854, 2017.

[21] X. Yue, Y. Liu, S. Kang, and A. Nallanathan, "Performance analysis of NOMA with fixed gain relaying over Nakagami-*m* fading channels," *IEEE Access*, vol. 5, pp. 5445–5454, 2017.

[22] T.-N. Tran and M. Voznak, "HD/FD and DF/AF with fixed-gain or variable-gain protocol switching mechanism over cooperative NOMA for green-wireless networks," *Sensors*, vol. 19, no. 8, p. 1845, Apr. 2019.

[23] İ. Altunbaş, A. Yılmaz, Ş. S. Kucur, and O. Kucur, "Performance analysis of dual-hop fixed-gain AF relaying systems with OSTBC over Nakagami-*m* fading channels," *AEU-Int. J. Electron. Commun.*, vol. 66, no. 10, pp. 841–846, Oct. 2012.

[24] M. Shirvanimoghaddam, M. Dohler, and S. J. Johnson, "Massive non-orthogonal multiple access for cellular IoT: Potentials and limitations," *IEEE Commun. Mag.*, vol. 55, no. 9, pp. 55–61, Sep. 2017.

[25] A. E. Mostafa, Y. Zhou, and V. W. S. Wong, "Connectivity maximization for narrowband IoT systems with NOMA," in *Proc. IEEE Int. Conf. Commun. (ICC)*, May 2017, pp. 1–6.

[26] Y. Liu, X. Li, F. R. Yu, H. Ji, H. Zhang, and V. C. M. Leung, "Grouping and cooperating among access points in user-centric ultra-dense networks with non-orthogonal multiple access," *IEEE J. Sel. Areas Commun.*, vol. 35, no. 10, pp. 2295–2311, Oct. 2017.

[27] K. Higuchi and A. Benjebbour, "Non-orthogonal multiple access (NOMA) with successive interference cancellation for future radio access," *IEICE Trans. Commun.*, vol. E98.B, no. 3, pp. 403–414, 2015.

[28] Y. Liu, Z. Ding, M. Eikashlan, and H. V. Poor, "Cooperative non-orthogonal multiple access in 5G systems with SWIPT," in *Proc. 23rd Eur. Signal Process. Conf. (EUSIPCO)*, Aug. 2015, pp. 1999–2003.

[29] Y. Ye, Y. Li, D. Wang, and G. Lu, "Power splitting protocol design for the cooperative NOMA with SWIPT," in *Proc. IEEE Int. Conf. Commun. (ICC)*, May 2017, pp. 1–5.

[30] Z. Hadzi-Velkov, I. Nikoloska, G. K. Karagiannidis, and T. Q. Duong, "Wireless networks with energy harvesting and power transfer: Joint power and time allocation," *IEEE Signal Process. Lett.*, vol. 23, no. 1, pp. 50–54, Jan. 2016.

[31] X. Lu, P. Wang, D. Niyato, D. I. Kim, and Z. Han, "Wireless networks with RF energy harvesting: A contemporary survey," *IEEE Commun. Surveys Tuts.*, vol. 17, no. 2, pp. 757–789, 2nd Quart., 2015.

[32] Z. Yang, Z. Ding, P. Fan, and N. Al-Dhahir, "The impact of power allocation on cooperative non-orthogonal multiple access networks with SWIPT," *IEEE Trans. Wireless Commun.*, vol. 16, no. 7, pp. 4332–4343, Jul. 2017.

[33] I. Krikidis, S. Timotheou, S. Nikolaou, G. Zheng, D. W. K. Ng, and R. Schober, "Simultaneous wireless information and power transfer in modern communication systems," *IEEE Commun. Mag.*, vol. 52, no. 11, pp. 104–110, Nov. 2014.

[34] E. Boshkovska, D. W. K. Ng, N. Zlatanov, and R. Schober, "Practical non-linear energy harvesting model and resource allocation for SWIPT systems," *IEEE Commun. Lett.*, vol. 19, no. 12, pp. 2082–2085, Dec. 2015.

[35] Y. Liu, L. Wang, T. T. Duy, M. Elkashlan, and T. Q. Duong, "Relay selection for security enhancement in cognitive relay networks," *IEEE Wireless Commun. Lett.*, vol. 4, no. 1, pp. 46–49, Feb. 2015.

[36] N.-P. Nguyen, T. Q. Duong, H. Q. Ngo, Z. Hadzi-Velkov, and L. Shu, "Secure 5G wireless communications: A joint relay selection and wireless power transfer approach," *IEEE Access*, vol. 4, pp. 3349–3359, 2016.

[37] L. J. Rodriguez, N. H. Tran, T. Q. Duong, T. Le-Ngoc, M. Elkashlan, and S. Shetty, "Physical layer security in wireless cooperative relay networks: State of the art and beyond," *IEEE Commun. Mag.*, vol. 53, no. 12, pp. 32–39, Dec. 2015.

[38] Z. Zhu, Z. Chu, Z. Wang, and I. Lee, "Outage constrained robust beamforming for secure broadcasting systems with energy harvesting," *IEEE Trans. Wireless Commun.*, vol. 15, no. 11, pp. 7610–7620, Nov. 2016.

[39] G. Pan, H. Lei, Y. Deng, L. Fan, J. Yang, Y. Chen, and Z. Ding, "On secrecy performance of MISO SWIPT systems with TAS and imperfect CSI," *IEEE Trans. Commun.*, vol. 64, no. 9, pp. 3831–3843, Sep. 2016.

[40] H. Lei, J. Zhang, K.-H. Park, P. Xu, I. S. Ansari, G. Pan, B. Alomair, and M.-S. Alouini, "On secure NOMA systems with transmit antenna selection schemes," *IEEE Access*, vol. 5, pp. 17450–17464, 2017.

[41] J. Zhu, Y. Zou, G. Wang, Y.-D. Yao, and G. K. Karagiannidis, "On secrecy performance of antenna-selection-aided MIMO systems against eavesdropping," *IEEE Trans. Veh. Technol.*, vol. 65, no. 1, pp. 214–225, Jan. 2016.

[42] A. Salem, K. A. Hamdi, and K. M. Rabie, "Physical layer security with RF energy harvesting in AF multi-antenna relaying networks," *IEEE Trans. Commun.*, vol. 64, no. 7, pp. 3025–3038, Jul. 2016.

[43] R. Zhao, Y. Yuan, L. Fan, and Y. He, "Secrecy performance analysis of cognitive decode-and-forward relay networks in Nakagami-*m* fading channels," *IEEE Trans. Commun.*, vol. 65, no. 2, pp. 549–563, Oct. 2017.
[44] L. Wang, M. Elkashlan, J. Huang, N. H. Tran, and T. Q. Duong, "Secure transmission with optimal power allocation in untrusted relay networks," *IEEE Wireless Commun. Lett.*, vol. 3, no. 3, pp. 289–292, Jun. 2014.
[45] G. Pan, C. Tang, T. Li, and Y. Chen, "Secrecy performance analysis for SIMO simultaneous wireless information and power transfer systems," *IEEE Trans. Commun.*, vol. 63, no. 9, pp. 3423–3433, Sep. 2015.
[46] A. A. Nasir, H. D. Tuan, T. Q. Duong, and H. V. Poor, "Secrecy rate beamforming for multicell networks with information and energy harvesting," *IEEE Trans. Signal Process.*, vol. 65, no. 3, pp. 677–689, Feb. 2017.
[47] K. M. Rabie, A. Salem, E. Alsusa, and M.-S. Alouini, "Energy-harvesting in cooperative AF relaying networks over log-normal fading channels," in *Proc. IEEE Int. Conf. Commun. (ICC)*, May 2016, pp. 1–7.
[48] T. D. P. Perera and D. N. K. Jayakody, "Analysis of time-switching and power-splitting protocols in wireless-powered cooperative communication system," *Phys. Commun.*, vol. 31, pp. 141–151, Dec. 2018.
[49] X. Chen, C. Yuen, and Z. Zhang, "Wireless energy and information transfer tradeoff for limited-feedback multiantenna systems with energy beamforming," *IEEE Trans. Veh. Technol.*, vol. 63, no. 1, pp. 407–412, Jan. 2014.
[50] B. Citoni, F. Fioranelli, M. A. Imran, and Q. H. Abbasi, "Internet of Things and LoRaWAN-enabled future smart farming," *IEEE Internet Things Mag.*, vol. 2, no. 4, pp. 14–19, Dec. 2019.
[51] T.-N. Tran and M. Voznak, "Switchable coupled relays aid massive non-orthogonal multiple access networks with transmit antenna selection and energy harvesting," *Sensors*, vol. 21, no. 4, p. 1101, Feb. 2021.
[52] T.-N. Tran, M. Voznak, P. Fazio, and V.-C. Ho, "Emerging cooperative MIMO-NOMA networks combining TAS and SWIPT protocols assisted by an AF-VG relaying protocol with instantaneous amplifying factor maximization," *AEU-Int. J. Electron. Commun.*, vol. 135, Jun. 2021, Art. no. 153695.
[53] X. Li, M. Zhao, M. Zeng, S. Mumtaz, V. G. Menon, Z. Ding, and O. A. Dobre, "Hardware impaired ambient backscatter NOMA systems: Reliability and security," *IEEE Trans. Commun.*, vol. 69, no. 4, pp. 2723–2736, Apr. 2021.
[54] H. Esmaiel, Z. A. H. Qasem, H. Sun, J. Qi, J. Wang, and Y. Gu, "Wireless information and power transfer for underwater acoustic time-reversed NOMA," *IET Commun.*, vol. 14, no. 19, pp. 3394–3403, Dec. 2020.

THANH-NAM TRAN was born in Vinh Long, Vietnam, in 1988. He received the M.Sc. degree from Military Technical Academy (MTA), in 2014. He is currently pursuing the Ph.D. degree in communications technology with the Faculty of Electrical Engineering and Computer Science, Technical University of Ostrava, Czech Republic. He works at Saigon University, Vietnam, as a Lecturer. He is also a Junior Researcher with the Research and Development Team of Prof. Miroslav Voznak at the Technical University of Ostrava. His major interests include NOMA, energy harvesting, cognitive radio, and physical layer security.

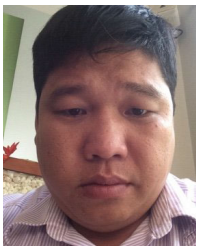

THOAI PHU VO was born in An Giang, Vietnam, in 1979. He received the M.E. degree from the Ho Chi Minh City University of Technology (HCMUT), in 2009, and the Ph.D. degree from Da-Yeh University (DYU), in 2015. He works at the Ton Duc Thang University, Vietnam, as a Lecturer and a Researcher with the Faculty of Electrical and Electronics Engineering, where he is also a Junior Researcher. His major interests include digital image processing, chip design with FPGA, fuzzy control, NOMA, energy harvesting, cognitive radio, physical layer security, and wireless sensor networks.

PEPPINO FAZIO was born in Italy, in 1977. He received the Ph.D. degree in electronics and communications engineering from the University of Calabria (UNICAL), Italy, in 2008. He completed his Habitation degree as an Associate Professor, in 2017, after being an Assistant Professor at the DIMES Department, UNICAL, until 2016. He is currently a Senior Researcher with the National Super Computing Centre, VSB-Technical University of Ostrava. He is main author or coauthor of over 100 articles indexed in Scopus/WoS. His research interests include mobile communication networks, QoS architectures and interworking, wireless and wired networks, mobility modeling for WLAN environments, mobility analysis for prediction purposes, routing, vehicular networking, MANET, and VANET. He is a peer reviewer and a TPC member of various international conferences and many international journals, including IEEE Transactions on Vehicular Technology, IEEE Communications Letters, *IEEE Vehicular Technology Magazine*, Springer *TELS*, *MONET*, Elsevier *VEHCOMM*, and *COMNET*.

MIROSLAV VOZNAK (Senior Member, IEEE) was born in Czechia, in 1971. He received the Ph.D. degree in telecommunications from the Faculty of Electrical Engineering and Computer Science, Technical University of Ostrava, in 2002. He completed his habitation in 2009, and was appointed as a Full Professor in electronics and communications technologies, in 2017. He is author or coauthor of more than 100 articles in SCI/SCIE journals. He served as the general chair for scientific conferences, such as IEEE/ACM DS-RT, in 2020, and IFIP WMNC, in 2018, and belongs to the World's Top 2% Scientists List by Stanford University. His research interests include information and communications technology, especially quality of service and experience, network security, wireless networks, and big data analytics.